Journal of Materials Chemistry B

ROYAL SOCIETY OF CHEMISTRY

REVIEW

View Article Online
View Journal | View Issue

Cite this: J. Mater. Chem. B, 2026, 14, 4816

Received 24th January 2026,
Accepted 14th March 2026

DOI: 10.1039/d6tb00194g

rsc.li/materials-b

Molecularly imprinted polymers as next-generation weapons against the AMR crisis

Ammar Ibrahim, *[ab] Alvaro Garcia,*[a] Amin M. Alrajhi*[c] and Sergey Pilestky *[a]

Antimicrobial resistance (AMR), referred to as the "Silent Pandemic", has become a massive threat to public health of the current and next generations. Molecularly imprinted polymers (MIPs) have emerged as a possible tool to fight AMR, due to their unique features, such as high affinity and specificity for relevant targets, easy manufacturing and good stability in physiological conditions. This review explores recent developments in combating AMR using MIPs as antibiotic drug carriers, using polymers for targeting components of the outer membrane of Gram-negative bacteria, blocking cell signalling by capturing quorum-sensing molecules, or binding alarmone nucleotide molecules.

Introduction

Antimicrobial resistance (AMR) is defined as the capacity of pathogens (such as bacteria, parasites, viruses, and fungi) to resist the effect of medicines, grow and continue in their pathogenic role,[1,2] which prolongs the treatment, or, in some cases, causes death to the infected patient. The incorrect use of antimicrobial drugs and the lack of public knowledge contribute to organisms developing the ability to resist drugs. Annually, 10 million deaths are expected due to AMR by 2050.[3] The extent of the problem has escalated to a high-risk level, with huge financing pressure upon healthcare organisations. In Europe, the annual estimation for AMR treatment is about 9 billion euros. Moreover, the Center for Disease Control and Prevention (CDC) has reported that AMR treatment costs in the USA are about 35 billion dollars per year.[4]

Antibiotics were the first common drugs applied and approved for microbial infection treatment. A wide range of antibiotics are still used, such as β-lactams, sulphonamides,[5] aminoglycosides,[6] tetracyclines,[7] lipopeptides,[8] oxazolidinones,[9] glycopeptides,[10] streptogramins,[11] macrolides,[12] lincosamides,[13] and quinolones.[14,15] They can kill microorganisms or curb their growth *via* various mechanisms, such as inhibiting cell wall synthesis or disrupting the cell wall structure, hindering protein synthesis through interaction with some ribosomes, affecting nucleic acid synthesis, and intervening in some metabolic pathways (Fig. 1). They have contributed to the eradication of many diseases and decreased the rate of fatalities in comparison with the pre-antibiotic era.[16] The ability of microorganisms to develop defences against antibiotics complicates the design and approval of new drugs. Thus, between 2010 and 2014, only four novel antibiotics were approved as new drugs.[17] In 2010, the World Health Organisation (WHO) classified antibiotic resistance as one of the three most dangerous threats to global health.[18] In 2021, WHO reported that "The antibacterial clinical and preclinical pipeline is stagnant and far from meeting global needs. Since 2017 only 12 antibiotics have been approved, 10 of which belong to existing classes with established mechanisms of antimicrobial resistance (AMR)".[19]

The primary challenge of AMR stems from the sophisticated array of resistance mechanisms that allow bacteria to withstand conventional antibiotic treatments, such as modification of penicillin-binding proteins (PBPs),[20–22] decrease of the cell membrane permeability,[23–25] pumping the drug outside the cell by efflux pumps,[26,27] or drug inactivation by β-lactamase enzymes.[28–30] This review provides a concise overview of bacterial resistance mechanisms and evaluates the evolution of molecularly imprinted polymers (MIPs) as a strategic tool against infection. Furthermore, it highlights specific bacterial cell membrane biomarkers as promising targets for the development of nanoparticles designed to disrupt essential survival pathways.

Nanotechnology and MIPs

In medicine, nanoparticles have become particularly valuable for disease detection, targeted therapy, and drug delivery. Their rational design has enhanced key characteristics such as bioavailability, compatibility, stability, and drug-loading capacity,

[a] Department of Chemistry, University of Leicester, Leicester, UK. E-mail: afii2@le.ac.uk, a.f.ibrahim89@gmail.com, agc14@leicester.ac.uk, sp523@leicester.ac.uk
[b] Ministry of Oil, North Refineries Company, Republic of Iraq
[c] Ministry of Environment, Water and Agriculture, Kingdom of Saudi Arabia. E-mail: e16907@mewa.gov.sa

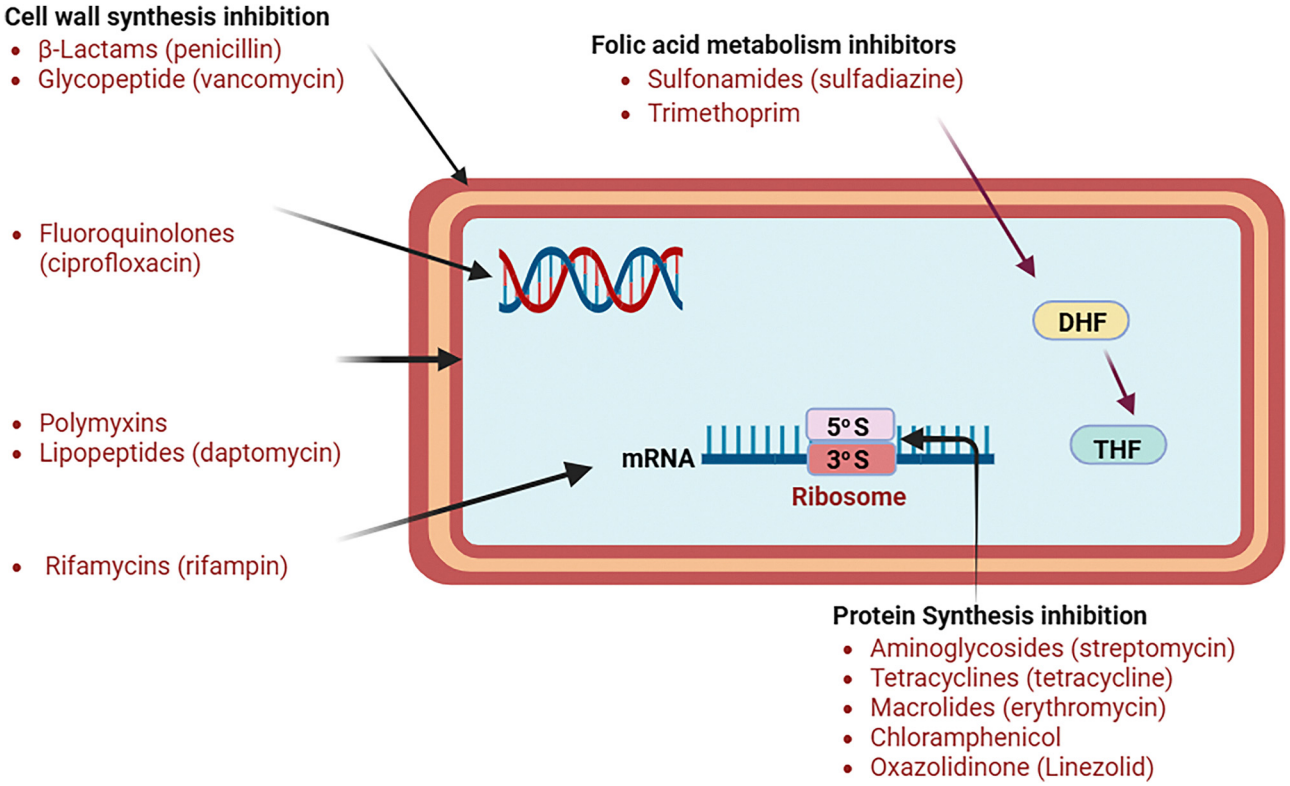

Fig. 1 Mechanisms of antibiotic action. DHF – dihydrofolic acid and THF – tetrahydrofolic acid. Reproduced from ref. 30 with permission from Elsevier, copyright (2021).

thereby extending their applications to gene therapy, tissue engineering, and diagnostic systems.[31] Among these systems, polymeric nanoparticles (PNPs) have received considerable attention because of their tunable properties, including morphology, shape, size (10–1000 nm), and molecular architecture.[32,33] Depending on the intended application, PNPs may be prepared either *via* direct polymerisation of monomers or from preformed polymers, with each approach producing particles of distinct size, encapsulation efficiency, and morphological features. This synthetic versatility offers researchers the ability to tailor nanoparticles for a broad spectrum of biomedical and industrial applications.[34]

Among polymeric nanomaterials, MIPs have emerged as a prominent class of synthetic materials distinguished by their ability to achieve highly specific molecular recognition. MIPs are defined as polymers that possess the ability to ''remember'' a target molecule through the formation of complementary binding sites generated during synthesis. This molecular memory allows selective rebinding of the template, mediated through covalent or non-covalent interactions, in a manner analogous to natural recognition systems.[35] The imprinting process involves the pre-assembly of a template with functional monomers, followed by polymerisation in the presence of a cross-linker, which stabilises the recognition cavities. The molecular imprinting process involves the copolymerisation of functional and cross-linking monomers in a solvent in the presence of a template molecule. Once polymerisation is complete, the template is removed, leaving specific recognition sites within the polymer structure. These imprinted cavities, which mirror the template in both geometry and chemical functionality, provide the material with the capacity for selective rebinding (Fig. 2).[36–38] MIPs can be synthesised through straightforward, cost-effective, and highly adaptable methods, such as precipitation polymerisation,[39,40] emulsion polymerisation,[41,42] core–shell imprinting,[43,44] and solid-phase methods,[45,46] enabling the production of micro- and nano-sized materials with excellent stability, robustness, selectivity, and biocompatibility.[47–49] Owing to these properties, MIPs have been successfully applied in a broad range of fields, including the recognition of amino acids and proteins.[50–53] nucleotide derivatives,[54] pollutants,[55,56] drugs and food,[57,58] chemical sensors,[59] catalysis,[60] drug delivery,[61] biological antibodies and receptor systems.[62,63]

MIPs as antimicrobials

MIPs have gained attention as promising synthetic recognition platforms with potential applications in antibacterial therapy. Over the past decade, MIPs have been investigated for bacterial cell recognition and antibacterial activity, reviewed by Tse Sum Bui *et al.*[64] Strategies have included imprinting entire bacterial cells[65–67] or selectively targeting key biomarkers located on the bacterial outer membrane. Such targets include lipopolysaccharides (LPS), which are essential components of Gram-negative

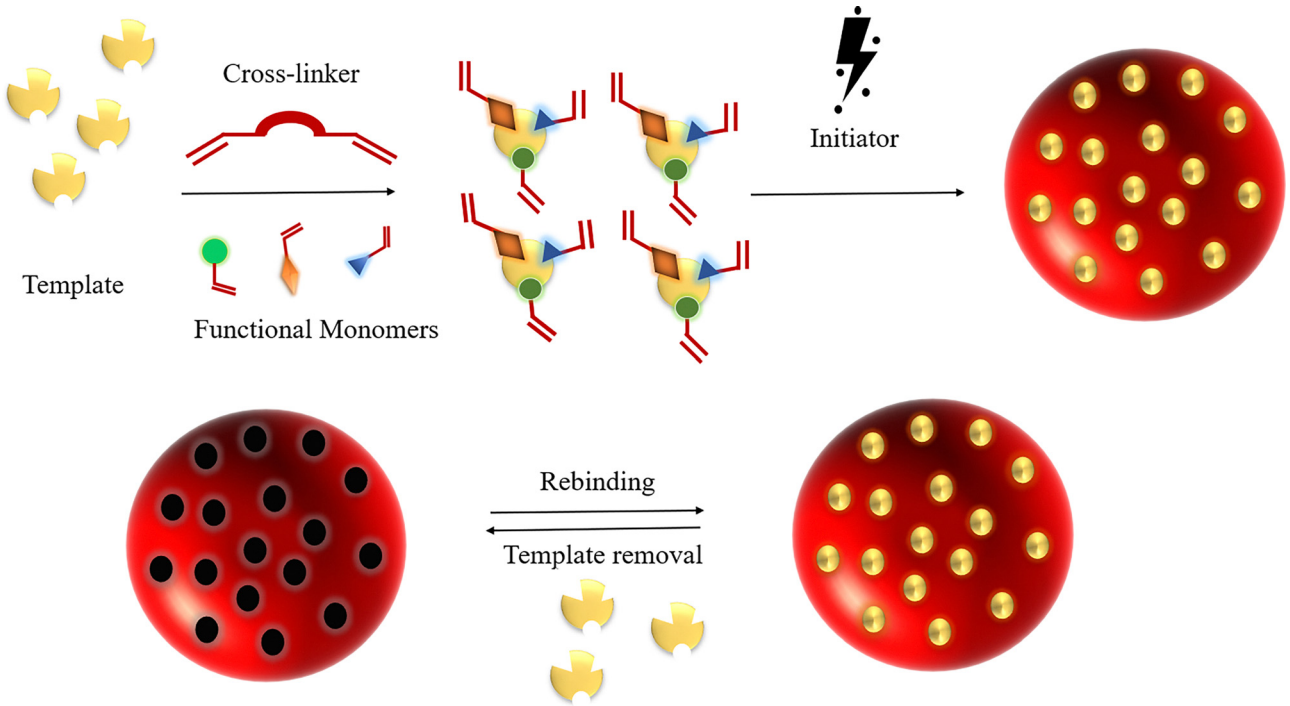

Fig. 2 Schematic illustration of the synthesis steps of molecularly imprinted polymer(s) (MIPs) and their rebinding performance.

cell walls,[68–71] quorum-sensing messengers, whose inhibition suppresses biofilm formation,[72–77] and drug-deactivating enzymes such as β-lactamase.[78] Other examples involve imprinting against flagellin,[79] a structural protein responsible for motility; protein A,[80] which mediates bacterial adhesion to host tissues and contributes to pathogenicity; and lipoprotein Lpp20,[81] a component implicated in outer membrane integrity and immune evasion. Furthermore, the integration of MIPs with conventional antimicrobial agents, such as MIP-loaded polymyxin B, has been demonstrated to enhance antibacterial activity against *Pseudomonas aeruginosa*.[82]

More recently, research has diversified into multiple therapeutic strategies in which MIPs are designed according to the nature of the bacterial biomarker and the chosen synthetic route. Table 1 summarises current advances in the development of MIPs for combating bacterial growth and resistance.

MIPs as drug delivery carriers

Bacterial eye infections, caused by pathogens such as *Pseudomonas aeruginosa*, *Staphylococcus aureus*, and *Escherichia coli*, are commonly treated through diverse therapeutic strategies. Among ocular drug delivery systems, soft contact lenses have attracted attention as potential carriers for sustained release of antibacterial agents. Ciprofloxacin (CFX), a fluoroquinolone antibiotic widely prescribed for corneal ulcers and bacterial eye infections, has been extensively employed in such systems. In this context, Kioomars *et al.*[83] reported the development of a molecularly imprinted polymer (MIP) hydrogel contact lens designed to combine the antibacterial activity of ciprofloxacin with the structural robustness of MIPs. Acrylamide monomers were used to synthesise the hydrogel matrix, enabling controlled loading and sustained release of CFX. Notably, the antibacterial effect increased over time, suggesting that the sustained release of CFX from the MIP network gradually disrupted bacterial defences.

In addition to its drug delivery function, the synthesised MIP hydrogel exhibited optical properties desirable for ophthalmic applications. It effectively absorbed a broad spectrum of ultraviolet (UV) radiation while maintaining approximately 85% transmission of visible light. This thereby provides both therapeutic and protective benefits. The study further identified reliable monomer-to-template ratios for optimised hydrogel synthesis, offering promising parameters for ocular drug loading and release. However, an important consideration is that both MIPs and NIPs displayed antibacterial effects against Gram-positive and Gram-negative strains. This raises potential concerns regarding the cytotoxicity of the polymer matrices themselves, which warrants careful evaluation of their safety for corneal, lens, and retinal tissues before clinical translation. The development of ciprofloxacin-loaded MIPs for the treatment of wound infections has been investigated by Galván Romero *et al.*[84] Their study demonstrated antibacterial activity against *Staphylococcus aureus* and *Escherichia coli*, with minimum inhibitory concentrations (MICs) ranging from 0.016 to 0.125 mg L^{-1} and 0.004 to 0.028 mg L^{-1}, respectively. Importantly, no cytotoxic effects were observed on fibroblast cells. These findings suggest that MIPs represent a promising strategy for the treatment of skin infections; however, further *in vivo* assessments are required.

Bacterial infections of bones and teeth, such as osteomyelitis or periodontitis, pose serious clinical challenges, particularly in the context of increasing AMR. Khademi and Kharaziha[85]

Table 1 Molecular imprinting strategies for fighting bacteria

MIP type	Applications	Therapy's target	Notes/outcomes	Targeted bacteria	Ref.
MIP-hydrogel	• Drug delivery (Ciprofloxacin)	Eye infections	• Sustained release • UV absorptivity	*P. aeruginosa*	83
Emulsion/bulk/ co-precipitation	• Drug delivery (Ciprofloxacin)	Skin/wound infections	• Lower drug dose • Sustained release	*E. coli*	84
Surface imprinting (bioglass–chitosan)	• Drug delivery (Doxycycline)	Osteomyelitis/ periodontitis	• Controlled release • Reduced cytotoxicity	*S. aureus*	85
MIP-alginate encapsulated	• Drug delivery (Vancomycin)	Wound dressing	• Controlled release • Clear inhibitory effect	*E. coli*	87
MIP-PVA/gelatine nanofibers	• Drug delivery (Gentamicin)	Wound dressing	• Slow release • Non-cytotoxic • Fast wound closure	*E. coli*	88
MIP-BC grafted	• Drug delivery (Gentamicin sulphate)	Broad spectrum	• Controlled release • Clear inhibitory effect	*S. aureus*	89
Boronic acid-supported MIP	• Boron affinity • Drug delivery (Chloramphenicol)	Inhibiting protein synthesis	• High bacterial killing effect	*E. coli*, *S. epidermidis*	90
Boronic acid-supported MIP	• Boron affinity • Photothermal therapy	Targeting LPS (cell wall)	• Remarkable affinity towards LPS • Selective recognition/inhibition	*E. coli*	91
MIP-AuNPs	• Photothermal therapy	Targeting LPS	• High affinity towards LPS • Selective bacterial inhibition	*E. coli*	92
MIP-homoserine lactone autoinducer	• Block quorum sensing	Biofilm formation	• Sequestration of signalling molecules • Reduced biofilm	MRSA, *P. aeruginosa*	73 and 75
MIP + z-pppGppp (Alarmone)	• Capture alarming nucleotides	Stress adaptation inhibition	• Effective *in vivo* dose reduction • Growth inhibition	*E. coli*	93
MIP-Lysozyme Cryogel	• Lysozyme release	Bacterial inhibition	• Constant release	*S. aureus*, *E. coli*	94
MIP-AgNPs	• Antibacterial	Cell wall disruption (β-linkage)	• Selective recognition • High antibacterial effect	*E. coli*, *S. epidermidis*	95
MIP-clindamycin (PU nanofibers)	• Drug delivery	Acne vulgaris	• Successful *in vivo* treatment • CFU reduction • No cytotoxic effect	*S. aureus*, *P. aeruginosa*, *K. pneumoniae*, *Proteus vulgaris*	96

developed an antibacterial and osteogenic treatment using surface imprinting to synthesise MIP-loaded doxycycline (DOX) over imprinted bioglass microspheres (BGMs) coated with chitosan. BGMs were synthesised *via* the sol–gel method,[86] followed by deposition of chitosan to produce chitosan-coated BGMs (BGMs@Cs). Acrylamide monomers were then polymerised over the BGMs@Cs in the presence of DOX as a template, which was subsequently removed by elution to form the final MIP structure (Fig. 3). *In vitro* antibacterial assays demonstrated that *Staphylococcus aureus* and *Escherichia coli* were resistant to BGMs@Cs-MIP and BGMs@Cs-NIP; however, the BGMs@Cs-MIP-DOX formulation exhibited a clear inhibition zone, confirming the antibacterial efficacy of the system. Cytotoxicity evaluation using MTT assay of MG63 cell-like osteoblast cells (bone-forming cells) displayed cell viability of more than 80% with BGMs@Cs-MIP and BGMs@Cs-NIP, which ensures the cytocompatibility of MIP and successful removal of unreacted acrylamide monomers that are known to have toxic and carcinogenic properties. Furthermore, the cytotoxicity of DOX can be avoided by encapsulation with MIP. Additionally, osteogenic differentiation assays demonstrated a significant increase in calcium deposition for MG63 osteoblast cells treated with BGMs@Cs-MIP-DOX compared to controls, confirming the bone-forming activity.

In another study focused on wound dressing development, MIPs were employed as drug carriers and incorporated into alginate, a naturally occurring polymer derived from seaweed commonly used in wound dressings. Kurczewska *et al.*[87] loaded the antibiotic vancomycin onto MIPs and subsequently encapsulated the vancomycin-loaded MIPs within an alginate matrix. MIPs were synthesised by combining vancomycin with the monomers ethylene glycol dimethacrylate and methacrylic acid, followed by initiation of the polymerisation reaction using potassium persulfate. The resulting MIPs were mixed with the alginate dressing and dried for 48 hours. *In vitro* release studies showed that vancomycin release from the MIP-alginate matrix was slower than from the control (Fig. 4), while antibacterial testing demonstrated that the inhibition zones against streptococcal strains were larger for vancomycin-MIP-alginate than for vancomycin-MIP alone. These findings highlight the potential of MIPs as antibiotic carriers, offering both controlled drug release and enhanced antibacterial activity.

MIPs exhibit promising characteristics that can effectively contribute to enhancing the performance of drug delivery systems, improving therapeutic outcomes, and optimising the pharmaceutical properties of drugs.

MIPs enhancing boron affinity to bacterial structures

Materials based on boronates exhibit a unique affinity for compounds and biomolecules containing *cis*-diol functionalities, such as nucleosides, saccharides, glycans, and glycoproteins, all of which are critical components of the cell surface. This distinctive property has been leveraged to develop a range of biological applications, including cell recognition[97–99] and the creation of antibacterial and anticancer drugs.[100–104] Prior research has integrated boronate affinity with MIPs for the selective recognition of various analytes: nucleosides in

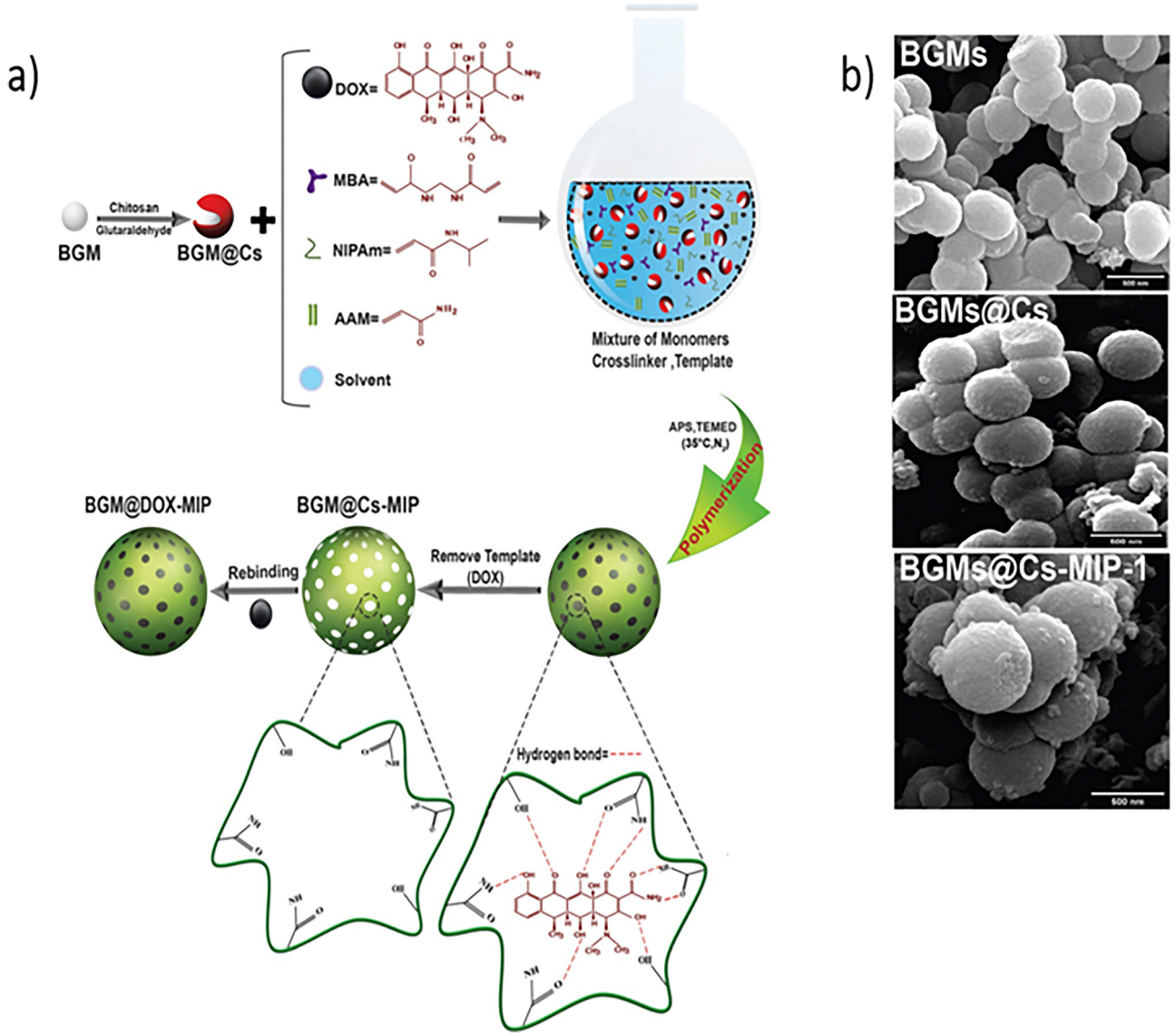

Fig. 3 (a) Schematic illustration of MIP synthesis over BGMs. (b) FE-SEM images of BGMs, coated chitosan (Cs) BGMs, and BGMs@Cs-MIP. Different surface roughness based on the particle formation stage. Reproduced from ref. 85 with permission from the American Chemical Society, copyright (2024).

pharmaceutical preparations,[105] glycoproteins, glycans, and monosaccharides,[106] as well as for the highly specific recognition of glucosides,[107] sialic acid,[108] and the rapid and selective isolation of luteolin.[109] Boronic acid moieties can bind to bacterial cell walls – specifically, to lipopolysaccharides in Gram-negative bacteria and peptidoglycans in Gram-positive bacteria.[110] This characteristic has been exploited to augment the antibacterial efficacy of chloramphenicol *via* MIPs. For example, Gong *et al.*[90] reported a novel approach to enhance chloramphenicol's antibacterial activity by synthesising MIPs through precipitation polymerisation. The synthesis involved the use of 3-(acrylamide)phenylboronic acid (APBA) and acrylamide monomers, with chloramphenicol serving as the template in an acetonitrile solvent. The incorporation of APBA introduced boronic acid groups into the MIP, enabling reversible boronate ester formation with bacterial cell wall components. The resulting MIP-loaded chloramphenicol demonstrated markedly improved antibacterial activity, with an IC_{50} of 0.6 μg mL^{-1} compared to 2 μg mL^{-1} for chloramphenicol alone. Moreover, the researchers observed a lower drug release at 37 °C (347 nm) relative to 20 °C (529 nm), establishing a clear correlation between particle size and drug release kinetics (Fig. 5).

Incorporation of boron-affinity functionality within MIPs significantly enhances their affinity for bacterial glycan structures while improving selectivity and stability under physiological conditions, ultimately leading to superior therapeutic system performance.

MIPs as photothermal antimicrobials

The selective detection of microorganisms through recognition of their characteristic biomarkers has emerged as an essential

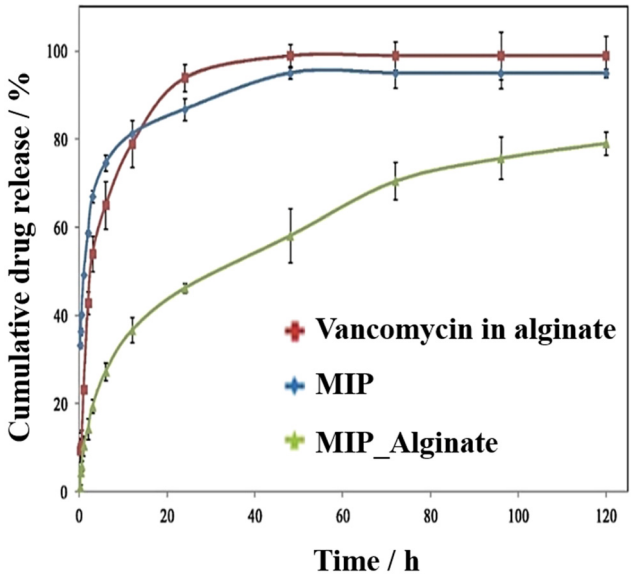

Fig. 4 Vancomycin release profiles from the encapsulated MIP in comparison to the controls. Reproduced the ref. 87 with permission from Elsevier, copyright (2017).

strategy in controlling pathogenic species such as bacteria, viruses, and fungi. Among the recently developed therapeutic approaches, photothermal therapy (PTT) has attracted considerable attention due to its high efficiency in various biomedical applications. PTT relies on the conversion of near-infrared (NIR) light into localised heat by nanomaterials situated within the disease microenvironment, thereby inducing damage to targeted cells.[111,112] Polydopamine nanoparticles (PDA NPs) are known for their biocompatibility, strong photothermal efficiency, and ability to interact with amino-containing molecules.[113] In a recent study, Zhang *et al.*[91] introduced a molecular imprinting strategy that integrates boronic acid affinity toward the bacterial outer membrane component lipopolysaccharide (LPS) with the photothermal properties of PDA NPs.

This approach enabled the specific recognition of LPS on the *Pseudomonas aeruginosa* cell membrane, followed by its inactivation *via* photothermal heating. For the synthesis, PDA NPs were first generated through the self-polymerisation of dopamine. In practice, PDA NPs were prepared and collected, and the boronic acid functionality was introduced using 4-formylphenylboronic acid and sodium cyanoborohydride. The next step involved the imprinting of LPS as a template molecule. LPS was immobilised onto the FPBA-functionalized PDA surface in phosphate buffer, followed by washing to remove any unbound LPS.

Subsequently, dopamine was added to initiate polymerisation, producing an outer polydopamine shell around the immobilised template. After 3 h of polymerisation at room temperature, the resulting photothermal molecularly imprinted polymers (PMIPs) were obtained (Fig. 6a). The photothermal performance of the PMIPs was assessed by exposing them to NIR irradiation. Within 10 min, the temperature of the PMIP suspension increased to 58.1 °C, a threshold sufficient to induce bacterial death. Control experiments revealed negligible antibacterial effects when *P. aeruginosa* was treated with either NIR alone or PMIPs without irradiation. In contrast, NIR-activated PMIPs reduced bacterial survival to below 1%. Fluorescence microscopy with SYTO9/PI dual staining, together with SEM imaging, confirmed severe membrane damage and apoptosis in *P. aeruginosa* cells following treatment with NIR-irradiated PMIPs (Fig. 6b–d).

Abiotic synthetic receptors are engineered materials designed to mimic the structure and function of natural biological receptors, enabling selective recognition and binding of target organisms. Despite their potential, the widespread application of abiotic synthetic receptors is limited by challenges related to synthesis complexity, cost, robustness, and adaptability to different environmental conditions. MIPs, as a class of synthetic receptors,[114] offer a promising alternative for achieving high specificity and stability. To optimise MIPs for bacterial recognition and treatment, Shao *et al.*[92] developed a rapid screening strategy to synthesise high-affinity, high-selectivity nano-MIPs. The screening was performed in a 96-well plate format, where monomers were combined at varying ratios in each row. The polymeric library was established from monomers comprising a variety of charged, neutral, and hydrophobic functional groups.

To prepare fluorescently labelled imprinted nanoparticles, the optimal monomer ratios, which exhibited the highest affinity constants (KD) towards LPS, namely 10% 1-vinylimidazole (IM), 10% *N*-[(3(dimethylamino)propyl]methylacrylamide, 30% *N*-*tert*-butylacrylamide (TBAm), 48% *N*-isopropylacrylamide (NIPAm), 2% *N*,*N*′-methylenebisacrylamide (BIS), and 2.5 mg of FITC, were selected for MIP synthesis. The prepolymerisation mixture included LPS template (2.5 mg), and the initiator ammonium persulfate (30 mg) dissolved in deionised water. Then, the polymerisation was performed at 65 °C for 1 h. Additionally, magnetic nanoparticles (10.4 mg) and gold nanorods (AuNRs) (1 mg) were incorporated to prepare magnetic imprinted nanoparticles (magnetic nano-MIPs) and AuNR@MIP composites with a similar optimal monomer ratio used to prepare the MIP under the same polymerisation conditions.

The resulting MIPs demonstrated remarkable performance. When cultured with *E. coli*, 95.3% of the bacteria were captured by magnetic nano-MIPs, compared to only 32.1% captured by non-imprinted magnetic nanoparticles (NIPs). In a more complex system, 97% of *E. coli* (10^5 cells per mL) in mouse whole blood were captured by magnetic nano-MIPs, whereas magnetic nano-NIPs captured only 62%, confirming the selectivity of the nano-MIPs in biological samples. The antimicrobial efficacy of the MIPs was further evaluated using photothermal treatment. Nano-MIPs encapsulated with AuNR@MIP were irradiated with a laser, resulting in highly efficient bacterial elimination. Compared with AuNR@NIPs, AuNR@MIPs demonstrated superior antimicrobial activity when co-cultured with mixed microbial populations, including *E. coli*, yeast, and *Bacillus subtilis*, highlighting their selectivity in complex bacterial environments (Fig. 7). These findings suggest that MIPs provide a cost-effective, stable, and highly selective alternative to conventional abiotic receptors, with significant potential for bacterial detection

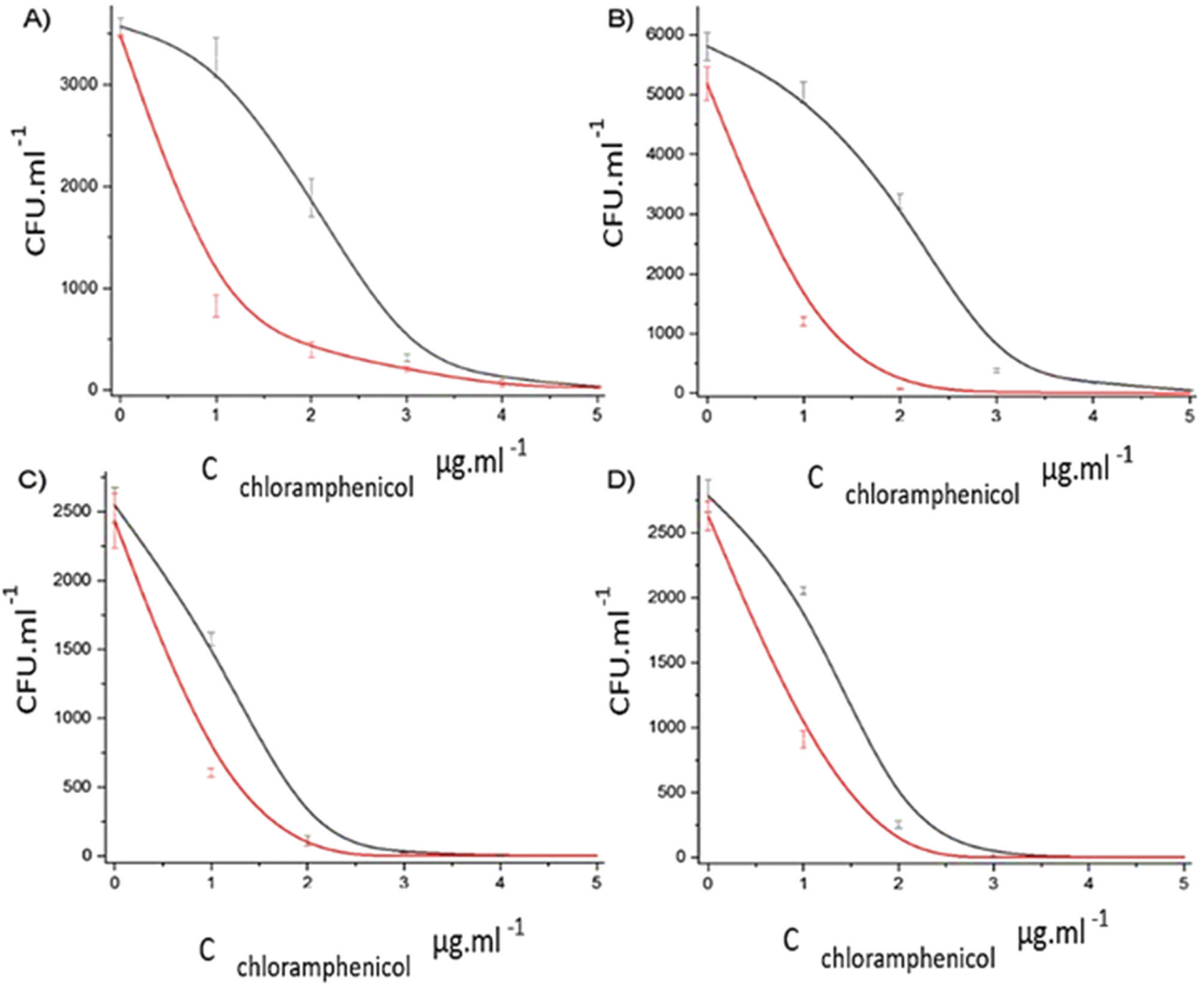

Fig. 5 Antibacterial effect of chloramphenicol (black) and chloramphenicol-loaded MIP2 (red) on *E. coli* (top) (A and B) and *S. epidermidis* (bottom) (C and D) at 37 °C (left) and 20 °C (right). Reproduced from ref. 90 with permission from John Wiley and Sons, copyright (2019).

and treatment applications. However, this approach needs to be further evaluated *in vivo* in animal experiments.

MIPs for blocking quorum-sensing molecules

Targeting the cellular mechanisms that sustain bacterial life offers an effective approach to suppressing bacterial growth. One of the most notable strategies employed by bacteria is quorum sensing (QS), a regulatory process through which gene expression is modulated in response to cell density. QS operates as a cell–cell signalling system that relies on the production, release, and detection of signalling molecules, known as autoinducers. These molecules accumulate in the surrounding environment during bacterial growth, and, in turn, promote biofilm formation and virulence, thereby enhancing bacterial survival. Biofilm development involves the adhesion of microorganisms to surfaces, followed by the formation of multicellular communities embedded within a protective extracellular matrix. Among the diverse classes of autoinducers, acyl-homoserine lactones (AHLs) are among the most extensively studied, as they readily diffuse across bacterial membranes and directly regulate gene expression.[115–118] Previous studies have investigated the sequestration of autoinducers using MIPs as a strategy to reduce biofilm formation.[72,119] In this context, Ma *et al.*[73] synthesised porous monolithic MIPs at the micrometre scale, employing *N*-(3-oxododecanoyl)-L-homoserine lactone (3-oxo-C12AHL) as the template, to inhibit *Pseudomonas aeruginosa* biofilm formation *via* autoinducer sequestration. These MIPs were prepared through bulk polymerisation using itaconic acid (IA) or 2-hydroxyethyl methacrylate (HEMA) as functional monomers, in the presence of ethylene glycol dimethacrylate (EGDMA) as the cross-linker and dimethylformamide (DMF) as the porogen solvent. Different template/monomer/cross-linker ratios (1 : 6 : 25, 1 : 6 : 48, 1 : 8 : 25, and 1 : 8 : 48) were employed. Polymerisation was initiated with an azo initiator under UV irradiation (365 nm, 6 W, with a 10 cm distance between the light source and the reaction solution) for 12 hours at 4 °C to prevent template degradation (Fig. 8). This method is simpler, cheaper, and requires less effort than

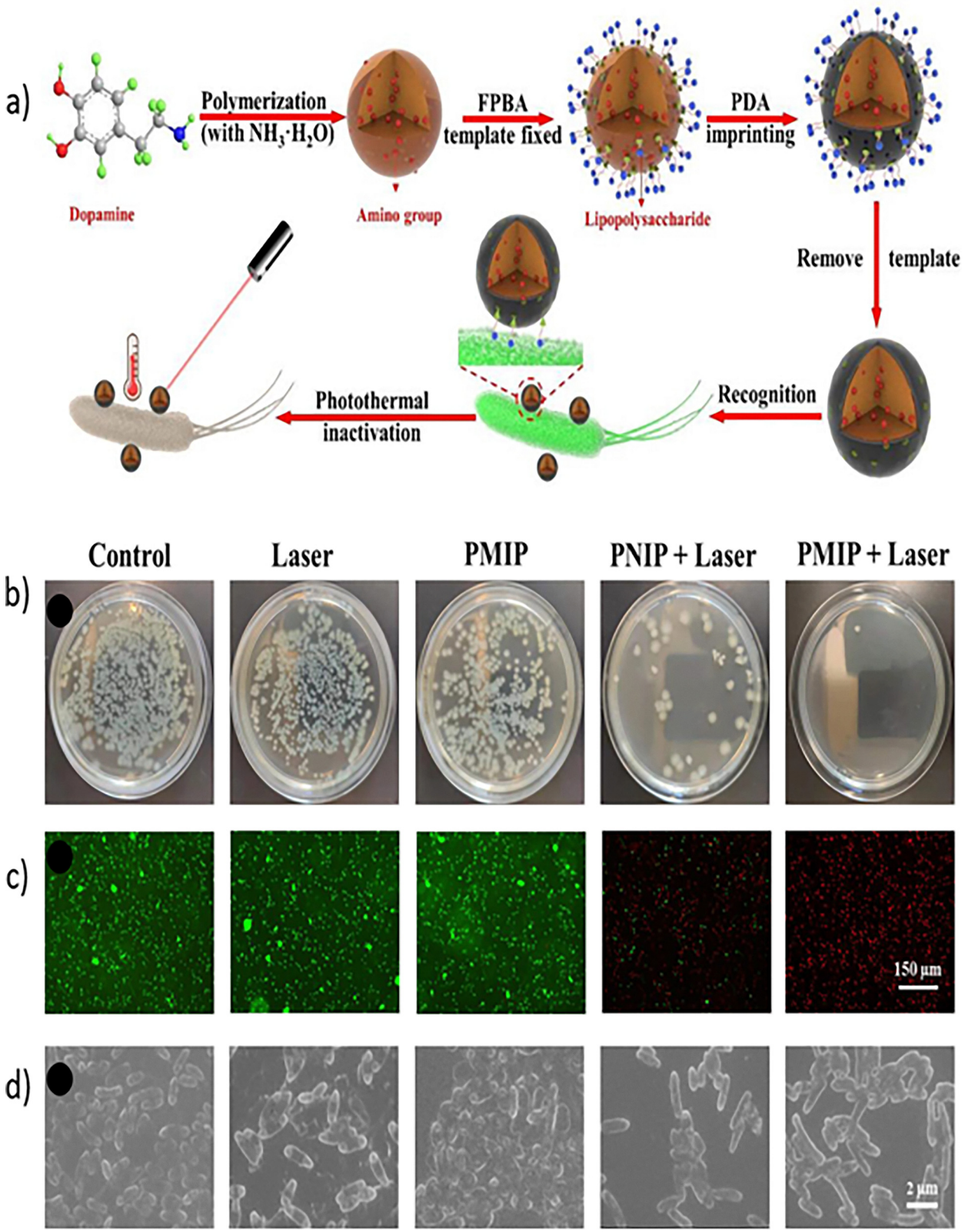

Fig. 6 (a) Schematic illustration of the preparation of PMIP. Different experimental groups of *P. aeruginosa* were tested with and without NIR and PMIP. (b) Bacterial colony photographs showing the bacteria's survival. (c) Fluorescent images of live/dead-stained bacteria. (d) SEM images. Reproduced from ref. 91 from the American Chemical Society under the terms of the Creative Commons CC-BY 4.0 (2023).

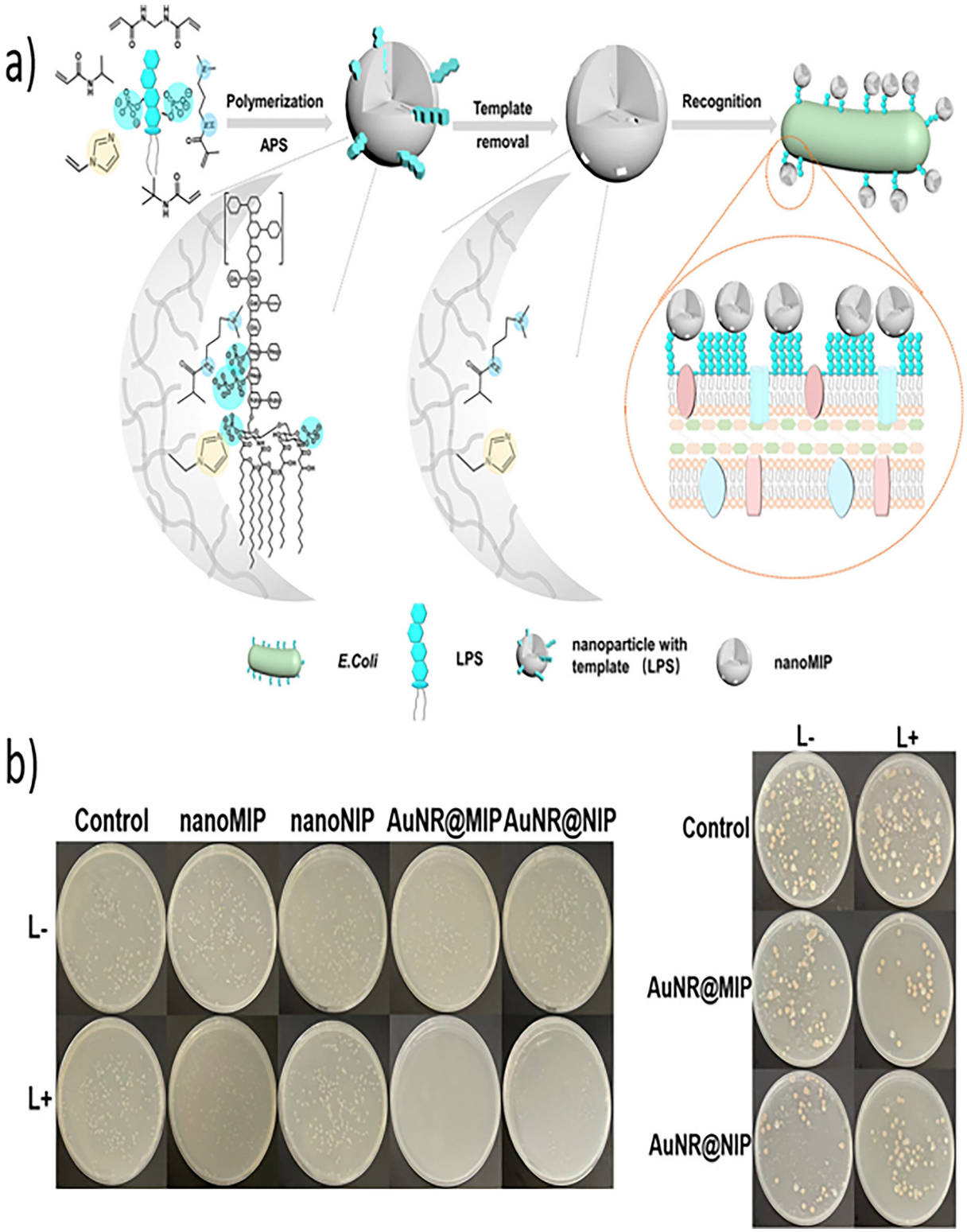

Fig. 7 (a) Schematic Illustration of the synthesis of MIP nanoparticles. (b) Photograph showing the PPT of *E. coli*, *B. subtilis*, and yeast incubated with AuNR@MIP and AuNR@NIP when treated with or without 808 nm laser irradiation. Reproduced from ref. 92 with permission from the American Chemical Society, copyrights (2023).

precipitation polymerisation and suspension polymerisation.[120] To evaluate biofilm inhibition, a crystal violet assay was performed to quantify the total biomass, while a triphenyl tetrazolium chloride (TTC) assay was conducted to assess cell viability. The antibiofilm activity results were consistent with the equilibrium rebinding data: HEMA-based MIPs, which

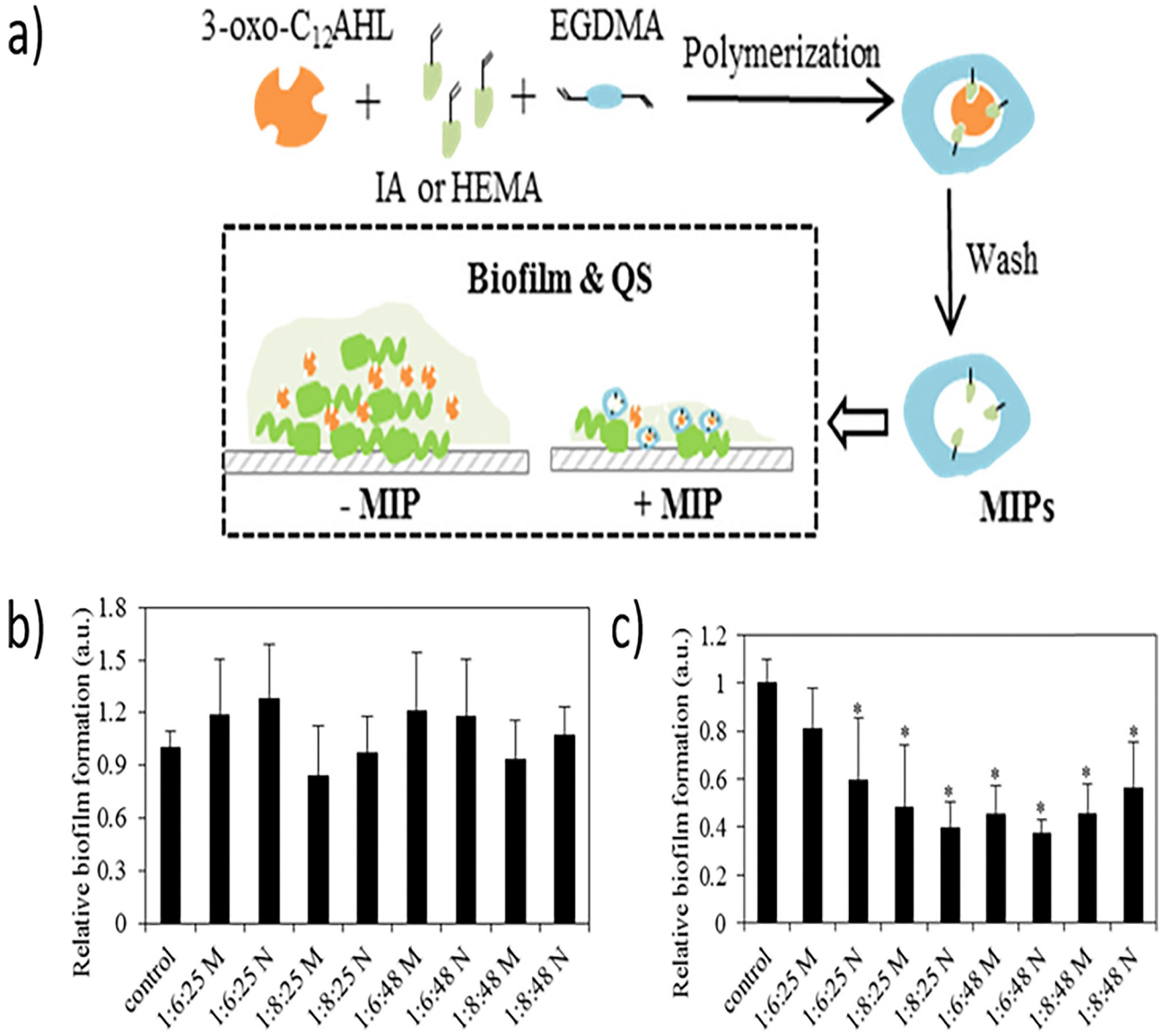

Fig. 8 (a) Schematic presentation of MIP development. Relative biofilm formation in the presence of (b) IA-MIPs and IA-NIPs and (c) HEMA-MIPs and HEMA-NIPs. Reproduced from ref. 73 with permission from the American Chemical Society, copyright (2018).

exhibited higher adsorption capacities than IA-based MIPs, demonstrated significant inhibition of biofilm formation (43.78–62.93%) compared with IA-MIPs and HEMA-NIPs.

Nevertheless, several limitations in this study merit attention. Although IA-MIPs adsorbed 3-oxo-C12AHL, they failed to suppress either biofilm formation or cell viability.

Furthermore, despite the promising inhibitory effects, no statistically significant difference was observed between HEMA-MIPs and their corresponding non-imprinted polymers (HEMA-NIPs). This raises critical questions regarding the imprinting quality achieved through bulk polymerisation, the optimisation of monomer-to-template ratios, and polymerisation conditions, particularly in comparison with other studies that reported more pronounced affinity differences between MIPs and NIPs.[72]

In the same area, Piletska and colleagues, in two consecutive studies,[72,121] explored the use of MIP-based microparticles to sequester AHL autoinducers and inhibit quorum-sensing pathways. However, their approach was limited by relatively low adsorption capacities. To address these shortcomings, López *et al.*,[75] working with the same research group, integrated Mosbach's transition state analogue (TSA) strategy for catalytically active MIPs[122] with the solid-phase synthesis protocol developed by Canfarotta *et al.*[45] This combination enabled the preparation of nano-MIPs capable of recognising and degrading the Gram-negative quorum-sensing autoinducer *N*-L-hexanoyl homoserine lactone (C6-AHL).

To design the TSA template, 6-amino-*N*-(1,1-dioxidotetrahydro-thiophen-2-yl)hexanamide was synthesised. This involved the preparation of 2-azidotetrahydrothiophene from 1-oxidotetrahydrothiophene *via* the Pummerer reaction, followed by its reaction with [*tert*-butyl-6-((1,1-dioxidotetrahydro-thiophen-2-yl)amino)-6-oxohexyl]carbamate, which was derived from

Boc-6-aminocaproic acid.[123] The TSA template was then immobilised onto activated glass beads *via* its amino group, after silanisation with (3-aminopropyl)triethoxysilane (APTMS). Six different nano-MIPs were subsequently synthesised using three different functional monomers; methacrylic acid (MAA), itaconic acid (IA), or 2-(dimethylamino) ethyl methacrylate (DEAEM) as functional monomers, together with the cross-linkers trimethylolpropane trimethacrylate and ethylene glycol dimethacrylate. The polymerisation mixture was added to 30 g of glass beads bearing the immobilised template and initiated under UV light using the "living" photoiniferter *N*,*N*′-diethyl dithiocarbamic acid benzyl ester. Dynamic light scattering (DLS) confirmed that the resulting TSA-nano-MIPs had particle sizes ranging between 175 and 204 nm, which represents a notable improvement compared to earlier MIP microparticles.

The hydrolytic activity of TSA-nano-MIPs toward the lactone ring of C6-AHL was investigated using liquid chromatography-mass spectrometry (LC-MS) by monitoring the decline in C6-AHL concentration over time. After 2 hours of incubation with 500 ng ml^{-1} of C6-AHL in water, TSA-nano-MIPs at 1 mg ml^{-1} achieved a 41% reduction in C6-AHL concentration, whereas non-specific nano-MIPs and controls without nano-MIPs showed reductions of only 17% and 0%, respectively. These findings confirm the successful imprinting of the TSA template and demonstrate the catalytic recognition activity. After 20 hours, the C6-AHL concentrations were reduced by approximately 57%, 31%, and 16% with MAA-TSA-nano-MIPs, non-specific nano-MIPs, and in the absence of nano-MIPs, respectively. Importantly, this work demonstrates that nano-MIPs can function as molecular recognition and catalytic systems at picomolar levels, a concentration range directly relevant to quorum-sensing environments, where autoinducer levels typically occur at the nanomolar scale.[124] Nevertheless, the translation of TSA-nano-MIPs into practical applications will require comprehensive assessments of their stability, functional performance, and scalability under biologically relevant conditions.

Beyond quorum sensing, bacteria employ another defence strategies to survive adverse environmental stresses such as nutrient deprivation and other harsh conditions. In these circumstances, bacteria produce signalling molecules known as alarmone nucleotides, namely guanosine 5′-diphosphate 3′-diphosphate (ppGpp) and guanosine 5′-triphosphate 3′-diphosphate (pppGpp), collectively referred to as (p)ppGpp. These small molecules play a central role in the stringent response, a global regulatory mechanism that enables bacteria to endure unfavourable conditions and maintain survival. Under normal conditions, cellular growth proceeds steadily, and alarmone levels remain low. However, under stress, their levels increase *via* synthetase activity, allowing cells to adjust by slowing growth to conserve nutrients and energy, while simultaneously enhancing antibiotic resistance and the expression of virulence factors.[125–127]

To assess whether nano-MIPs could interfere with this adaptive response, Chen *et al.*[93] developed molecularly imprinted nanoparticles using guanosine-5′-diphosphate disodium salt (ppG) as a template. The template was immobilised onto silanised glass beads, and nano-MIPs were synthesised through a solid-phase protocol employing *N*-isopropylacrylamide (NIPAm, 1.6 mmol), *N*-(3-aminopropyl) methacrylamide hydrochloride (APM, 0.2 mmol), *N*-*tert*-butylacrylamide (TBAm, 0.1 mmol), and *N*,*N*′-methylenebisacrylamide (Bis, 0.1 mmol) as a cross-linker. Polymerisation was carried out in 48 mL of water and initiated by potassium persulfate (KPS, 18 mg in 500 μL water) and tetramethylethylenediamine (TEMED, 1.3 μL).[45] The synthesised nano-MIPs demonstrated excellent biocompatibility. When incubated with sheep red blood cells (RBCs), the haemolysis rate was below 5%, while cytotoxicity assays with Madin–Darby canine kidney (MDCK) cells indicated cell viability above 89%, confirming their safety for biological applications. The antimicrobial activity of these nano-MIPs was then evaluated against both Gram-negative bacteria (*E. coli* and *kanamycin-resistant E. coli*) and Gram-positive bacteria (*S. aureus* and *MRSA*). Their ability to capture stress-induced signalling molecules was tested following stimulation either by UV radiation (254 nm) or antibiotics; oxytetracycline hydrochloride (OTC), or Kanamycin sulfate (KS).

Notably, the combination of nano-MIPs with antibiotics; demonstrated greater inhibitory efficiency compared to the full dose of the antibiotic alone, with the results showing a clear inhibition rate-concentration dependency. The therapeutic potential of the nano-MIPs was further validated *in vivo* using a wound infection model in male Balb/c mice (6–7 weeks old, 18–20 g). Twelve mice were inflicted with 8 × 8 mm dorsal wounds inoculated with *E. coli* (10 μL, 1.0×10^8 CFU mL^{-1}). After 24 hours, the animals were divided into four groups: negative control (saline 0.9%), nano-MIPs, positive control (oxytetracycline [OTC], 10 μL, 1.0 mg mL^{-1}), and a combination therapy (OTC 5 μL, 0.1 mg mL^{-1} + nano-MIPs 5 μL, 0.05 mg mL^{-1}). After six days of treatment, wound shrinkage was 65% and 68% in the OTC and OTC + nano-MIP groups, respectively, whereas only 31% and 30% shrinkage was observed in the negative control and nano-MIP-only groups. Bacterial colony counts from harvested wound tissues further confirmed that the lowest bacterial loads were observed in the OTC and OTC + nano-MIP groups. Overall, this study demonstrated that nano-MIPs can enhance the antibacterial effects of conventional antibiotics, enabling the same therapeutic outcomes with only half the effective drug dose. This highlights their potential role in reducing antibiotic consumption while maintaining efficacy.

Other strategies using MIPs to fight bacteria

Cryogel-based polymers, owing to their highly porous architecture, mechanical stability, and capacity to act as biomolecule carriers, have attracted considerable attention for antimicrobial applications.[128] Employing a molecular imprinting technology (MIT) approach, Gür *et al.*[94] synthesised a lysozyme-imprinted cryogel membrane (MIP-Lyz) designed for antibacterial activity against both Gram-positive and Gram-negative bacteria. Lysozyme (Lyz) is a small, naturally occurring globular protein[129] with well-established antibacterial activity through hydrolysis of the β-1,4 glycosidic linkages in the peptidoglycan layer of Gram-positive bacteria.[130] Its effect against Gram-negative

bacteria is comparatively limited due to the protective outer membrane;[131,132] however, Lyz can destabilise this barrier in the presence of divalent metal ions, such as Cu^{2+}, which act as membrane-permeabilising cofactors. To exploit this mechanism, the authors employed *N*-methacryloyl-(L)-histidine methyl ester (MAH) complexed with Cu^{2+} to improve the interaction between MAH and lysozyme.

The cryogel was prepared using 2-hydroxyethyl methacrylate (HEMA) as a functional monomer, *N*,*N*′-methylene bisacrylamide (MBAAm) as the cross-linker, and ammonium persulfate (APS) with tetramethylethylenediamine (TEMED) as initiators. Polymerisation was carried out between two glass plates at −12 °C for 24 hours, resulting in a lysozyme-imprinted cryogel membrane. Antibacterial evaluation demonstrated that the MIP-Lyz cryogel produced distinct zones of inhibition against both *Staphylococcus aureus* (Gram-positive) and *Escherichia coli* (Gram-negative). Interestingly, the cryogel exhibited stronger and more rapid activity against *E. coli* than *S. aureus*, highlighting its potential to overcome the outer membrane barrier of Gram-negative bacteria. In contrast, the corresponding non-imprinted cryogel (NIP) showed a negligible antibacterial effect, confirming that the activity arose from specific lysozyme adsorption and release.

Further assays revealed that antibacterial performance was concentration-dependent: higher lysozyme loading in the MIP-cryogel correlated with enhanced inhibition, reflecting a sustained release of Lyz from the cryogel matrix. The cytotoxicity of both MIP and NIP cryogel membranes was evaluated using the mouse fibroblast cell line L929. After 24 hours of incubation, cell viability assays confirmed that the synthesised cryogels were non-cytotoxic, indicating their biocompatibility and suitability for biomedical applications. Collectively, these findings demonstrate that lysozyme-imprinted cryogels provide a promising platform for controlled antimicrobial delivery, with particular efficacy against Gram-negative pathogens.

Nanofibers are widely recognised for their intrinsic advantages, including large surface area, high porosity, and low production cost, which collectively provide excellent drug-loading capacity.[133] However, conventional nanofiber systems face challenges in achieving controlled drug release, a limitation that can be mitigated through polymer grafting strategies.[134,135] Among these systems, bacterial cellulose (BC) nanofibers, biosynthesised by *Acetobacter xylinum*, have emerged as highly effective drug carriers due to their biocompatibility, mechanical strength, and efficient loading properties.[136,137]

To combine the molecular recognition ability of MIPs with the carrier advantages of nanofibers, Tamahakar *et al.*[89] developed a controlled drug loading and release platform by grafting MIP microparticles onto BC nanofibers through *in situ* polymerisation. In their approach, methacrylic acid (MAA) was employed as the functional monomer, *N*,*N*′-methylene bisacrylamide (MBAAm) as the cross-linker, and gentamicin sulfate, a broad-spectrum antibiotic, as the template, and 2,2 azobis(2-methylpropionitrile) as the initiator. BC nanofibers were extracted from *A. xylinum* (strain 10245). Three MIP formulations were prepared using a fixed ratio of MAA (1 mmol) and MBAAm (1 mmol), with varying gentamicin concentrations (0.20, 0.10, and 0.05 mmol).

Drug loading and release experiments showed that the imprinting method was successful, with results strongly influenced by the amount of gentamicin used during polymerisation. MIPs prepared with higher gentamicin concentrations were able to load more of the drug. In terms of release, the MIPs provided a slower and more controlled profile compared to non-imprinted polymers (NIPs). While NIPs released almost all (98%) of their gentamicin within just 8 hours, the release from MIPs was more gradual: MIP1 (the highest gentamicin concentration) released about 97% in 48 hours, MIP2 released around 80%, and MIP3 about 60% in the same period. This difference is explained by the formation of recognition cavities during polymerisation, which regulate how much drug can be loaded and how slowly it is released, depending on the template concentration used. The antibacterial activity of the MIP–nanofiber composites was assessed against Gram-negative *E. coli* and Gram-positive *S. aureus*. The inhibition zones produced by MIP1, MIP2, and MIP3 were 11.0, 9.5, and 7.5 mm for *E. coli*, and 14.5, 13.5, and 12.5 mm for *S. aureus*, respectively. These results confirmed concentration-dependent antibacterial activity, with higher template loading translating into more effective inhibition. Overall, the findings highlight MIP-functionalised BC nanofibers as a promising therapeutic platform, offering sustained antibiotic release and effective antibacterial activity, with performance adjustable through the drug concentration applied during polymerisation.

Nanofiber-based scaffolds in combination with gentamicin-imprinted polymers have also been explored for antibacterial applications, particularly in wound healing. Wound dressings play a critical role in skin regeneration, as wounded tissue provides a favourable environment for colonisation and proliferation of a wide range of microorganisms. Among various biomaterials, polyvinyl alcohol (PVA) and gelatin are frequently employed in tissue engineering due to their biocompatibility and biodegradability.[138,139] Building on these properties, Koudehi and Ziaseresht[88] developed MIP-based wound dressing by fabricating gentamicin-imprinted PVA/gelatin nanofibers through electrospinning. The polymerisation involved a cross-linking reaction between the hydroxyl groups of PVA and the aldehyde groups of glutaraldehyde, catalysed by hydrochloric acid.[140] Following polymerisation, the gentamicin template was removed *via* Soxhlet extraction, and the MIPs were subsequently reloaded with the drug. Drug release studies revealed a clear difference between MIP- and non-imprinted polymer (NIP)-based nanofibers. While approximately 85% of gentamicin was released from the NIP system within the first 8 hours, the PVA/gelatin/MIP nanofibers exhibited a significantly slower and more controlled release profile, with only 50% release after 40 hours and complete (98%) release after 110 hours. Importantly, the MIP nanofibers demonstrated no cytotoxicity against fibroblast cells, confirming their biocompatibility. The therapeutic efficacy was further validated *in vivo* using a rat skin wound model. Full-thickness excision wounds (8 mm) were treated with PVA/gelatin/MIP nanofibers, PVA/gelatin

nanofibers, or left untreated (control). After 14 days, wounds treated with MIP nanofibers exhibited complete skin regeneration, whereas those treated with non-imprinted nanofibers or left untreated showed only partial healing, with wound sizes reduced to approximately 5 mm and 2 mm, respectively. Taken together, this study exemplifies the broader potential of integrating molecular imprinting with nanofiber-based scaffolds to design multifunctional wound dressings that combine controlled antibiotic release, selective recognition, and tissue compatibility.

In a similar area, *Acne vulgaris* is a common dermatological condition associated with dysbiosis of the skin microbiota, particularly the overgrowth of acne-associated bacteria, and is clinically characterised by pimples, comedones (whiteheads and blackheads), and chronic inflammation of the sebaceous follicles.[141] Conventional treatment strategies rely on the administration of topical and oral antibiotics, among which clindamycin (Cln) is one of the most widely prescribed topical agents. However, challenges such as limited drug penetration, reduced bioavailability, and the emergence of resistance often compromise therapeutic outcomes. To address these limitations, Elhabal *et al.*[96] designed a nano-MIP-based drug delivery system aimed at enhancing the antibacterial activity of clindamycin. In their work, Cln-MIPs were synthesised *via* precipitation polymerisation at 60 °C using methacrylic acid (MAA, 4 mmol) as the functional monomer, ethylene glycol dimethacrylate (EGDMA, 20 mmol) as the cross-linker, methanol as the porogenic solvent, and AIBN as the radical initiator. The resulting Cln-MIPs were subsequently incorporated into polyurethane nanofiber scaffolds (PUNFs) at a loading of 14% using electrospinning. Successful deposition of Cln-MIPs was confirmed by measurable increases in both scaffold thickness (from 0.18 mm to 0.28 mm) and weight (from 22.65 mg to 31.54 mg). *In vivo* evaluations demonstrated that Cln-MIP-loaded PUNFs were non-toxic and exhibited superior therapeutic efficacy compared with Cln-MIPs alone or clindamycin controls. Specifically, Cln-MIP-PUNFs markedly reduced redness and inflammation in infected rat ears, while also achieving a significant reduction in *S. aureus* colonization – from $\sim 1 \times 10^8$ CFU mL^{-1} in untreated controls to 3.9×10^2 CFU mL^{-1} in the treated group (Fig. 9). By comparison, positive (clindamycin) controls resulted in 9.2×10^3 CFU mL^{-1}, highlighting the enhanced antibacterial performance of the MIP-functionalised nanofiber system. This innovative approach underscores the potential of integrating nano-sized MIP carriers with nanofiber scaffolds to improve topical antibiotic delivery. By enhancing drug permeability, prolonging release, and reducing bacterial load, such systems provide compelling evidence for the therapeutic applicability of MIP-based platforms in treating skin infections such as acne vulgaris.

Surface-imprinted polymers represent a versatile strategy for bacterial recognition and control, offering the ability to combine selective targeting with antimicrobial functionality. Gong *et al.*[95] introduced an innovative approach by fabricating silver nanoparticle (AgNP)-embedded surface-imprinted polymer beads (Ag-BIBs) through an oil-in-water pickering emulsion polymerisation method. Silver nanoparticles were incorporated owing to their broad-spectrum antibacterial properties,[142] which have a well-known bactericidal effect by disrupting the cell membrane structure and functions in Gram-negative bacteria. In this study,

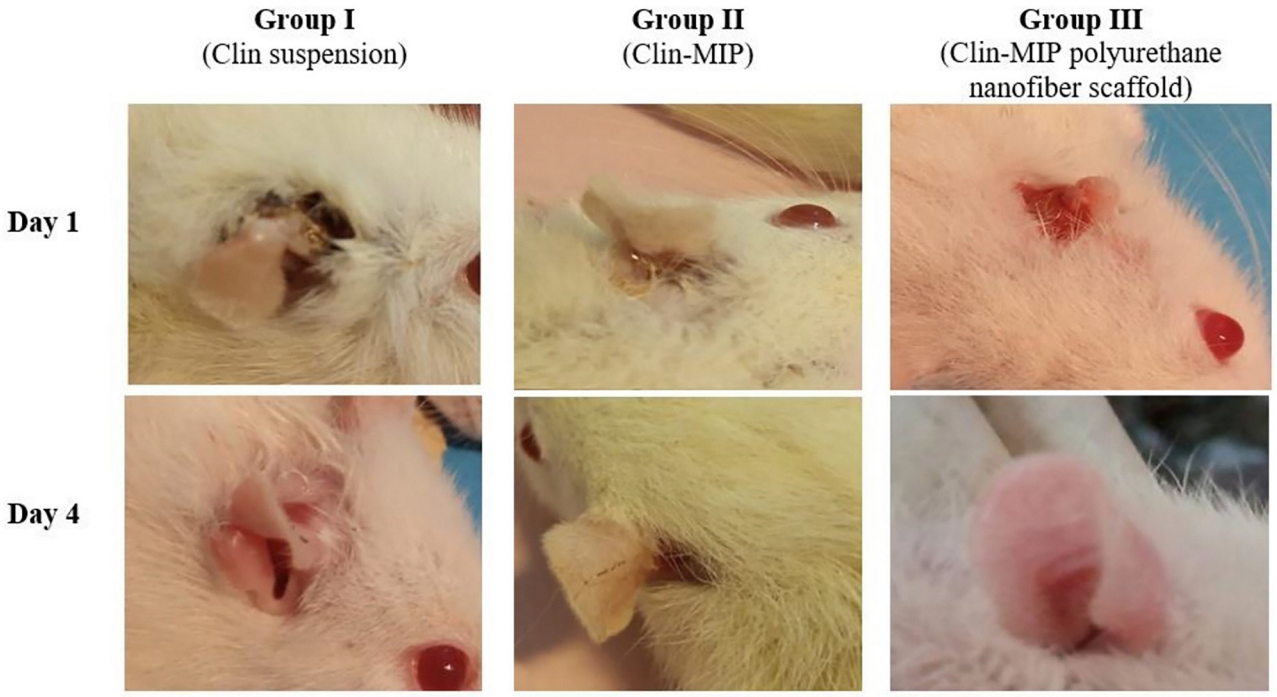

Fig. 9 Antibacterial activity of clindamycin and Clin-MIP polyurethane nanofibers against *S. aureus* (ATCC 6538) for different time intervals. Reproduced from ref. 96 under the terms of the Creative Commons CC BY license (MDPI) (2024).

E. coli (TG1, rod-shaped, Gram-negative) and *S. epidermidis* (PCI 1200, spherical, Gram-positive) were employed as templates to prepare bacteria-imprinted beads (BIBs). The Ag-BIBs were fabricated by combining a water phase containing bacteria pre-coated with an acrylate-functionalised polyethyleneimine prepolymer with an oil phase consisting of Ag nanoparticles, trimethylolpropane trimethacrylate (TRIM), divinylbenzene (DVB), and the initiation mixture of benzoyl peroxide (BPO) and *N*,*N*-dimethylaniline (DMA) in hexane (Fig. 10a). Binding assays demonstrated that the optimised Ag-BIBs exhibited pronounced bacterial recognition and capture efficiency, achieving up to 50% binding of *E. coli* and 60% of *S. epidermidis* in PBS, and as high as 90% for both species in LB medium.

Antibacterial testing further confirmed that the captured bacteria displayed markedly impaired growth in LB in the presence of Ag-BIBs. This bactericidal activity was attributed to the dual action of the imprinted beads: (i) selective recognition and capture of the bacterial targets, and (ii) the subsequent release of Ag nanoparticles embedded within the polymer matrix, which disrupt bacterial membranes. Interestingly, the release of Ag^+ ions into aqueous solution remained below 11% of the total Ag content, indicating that the antibacterial effect was largely governed by an Ag-BIB surface-mediated contact mechanism rather than extensive ion leaching into the medium. This feature is particularly advantageous as it minimises unnecessary silver release, thereby reducing potential environmental and cytotoxic risks while maintaining strong antibacterial efficacy.

Promising bacterial proteins as recognisable biomarkers to MIPs for future works

In this section, we discuss the potential of MIPs to target bacterial proteins that play a pivotal role in microbial survival and resistance. Bacterial persistence and drug resistance are mediated by diverse biochemical mechanisms, many of which rely on proteins essential for growth and adaptation. A notable example is β-lactamases, a broad family of bacterial enzymes responsible for conferring resistance to β-lactam antibiotics (*e.g.*, penicillins, cephalosporins, and carbapenems) by hydrolysing the β-lactam ring and thereby abolishing its inhibitory effect on cell wall synthesis. These enzymes are widely expressed in clinically relevant pathogens, including *Pseudomonas aeruginosa*, *Klebsiella pneumoniae*, and *E. coli*.[143,144]

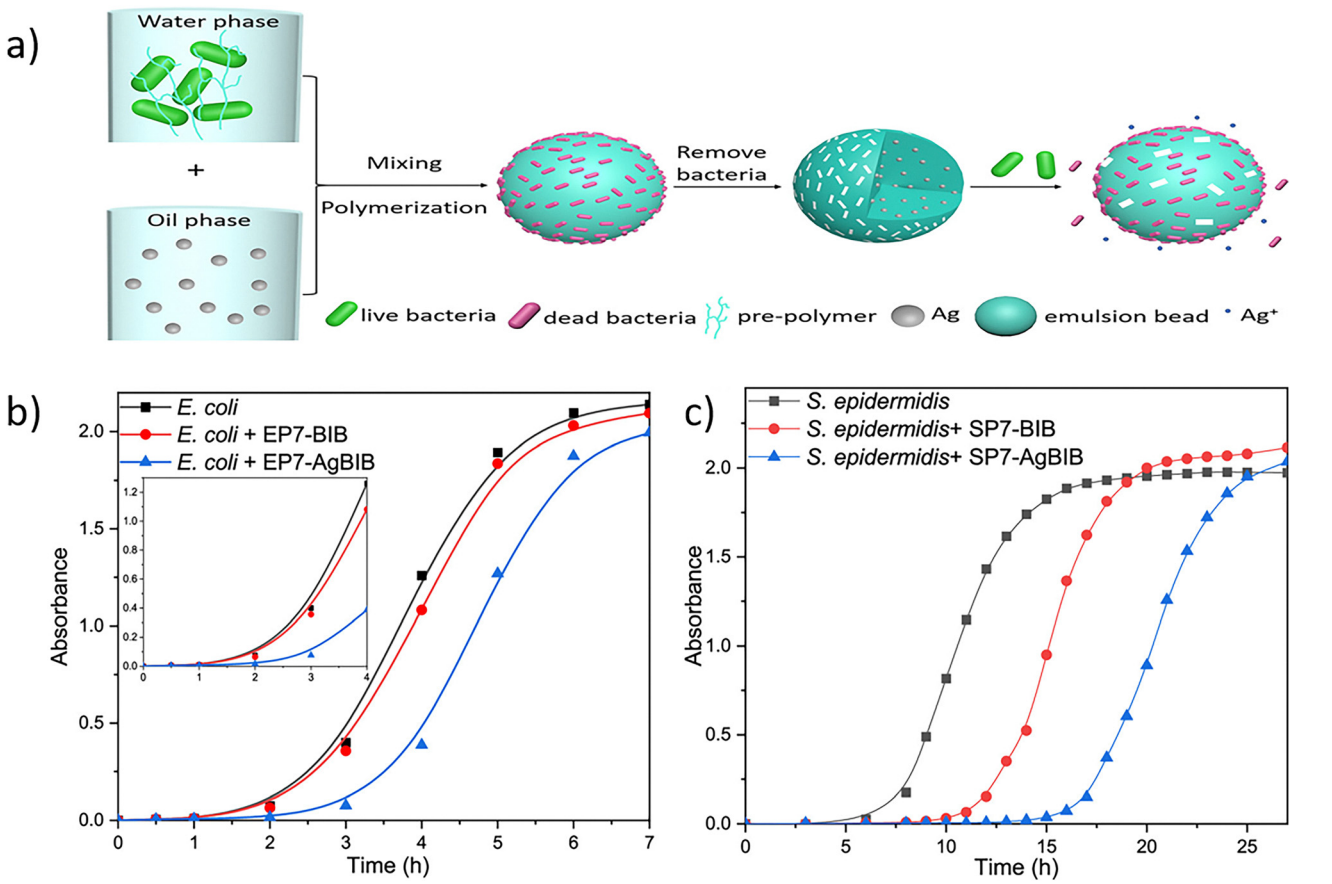

Fig. 10 (a) Schematic illustration of Ag-MIPs. Growth curves of *E. coli* (b) and *S. epidermidis* (c) in L.B. medium in the presence of bacteria-imprinted polymers with and without Ag loading. Reproduced From ref. 95 from the American Chemical Society under the terms of the Creative Commons CC-BY 4.0 (2023).

Table 2 Examples of bacterial outer membrane structures

Outer membrane proteins	Function	Structure	Ref.
OmpF porin	Allows diffusion of small hydrophilic molecules such as nutrients and waste products across the outer bacterial membrane	β-Barrel	146 and 147
LamB porin	Facilitates the diffusion of maltose and maltodextrin into the cell	β-Barrel	148 and 149
BtuB outer membrane protein	Transporter that permits the high-affinity binding and transport of vitamin B_{12}	β-Barrel protein	150 and 151
TolC outer membrane protein	Channel for Type I secretion systems (T1SS)	β-Barrel protein	152
LptD/LptE outer membrane proteins	Translocates LPS across the outer membrane to the outer leaflet	β-Barrel protein complex	153 and 154
BamA β-barrel assembly machinery protein	Assembly and insertion of outer membrane proteins (OMPs) and maintaining membrane integrity	β-Barrel protein	155 and 156

Li *et al.*[78] successfully demonstrated the feasibility of the approach, employing β-lactamase as a template for the preparation of stimuli-responsive imprinted hydrogels *via* free-radical polymerisation of low-cost monomers. When tested against

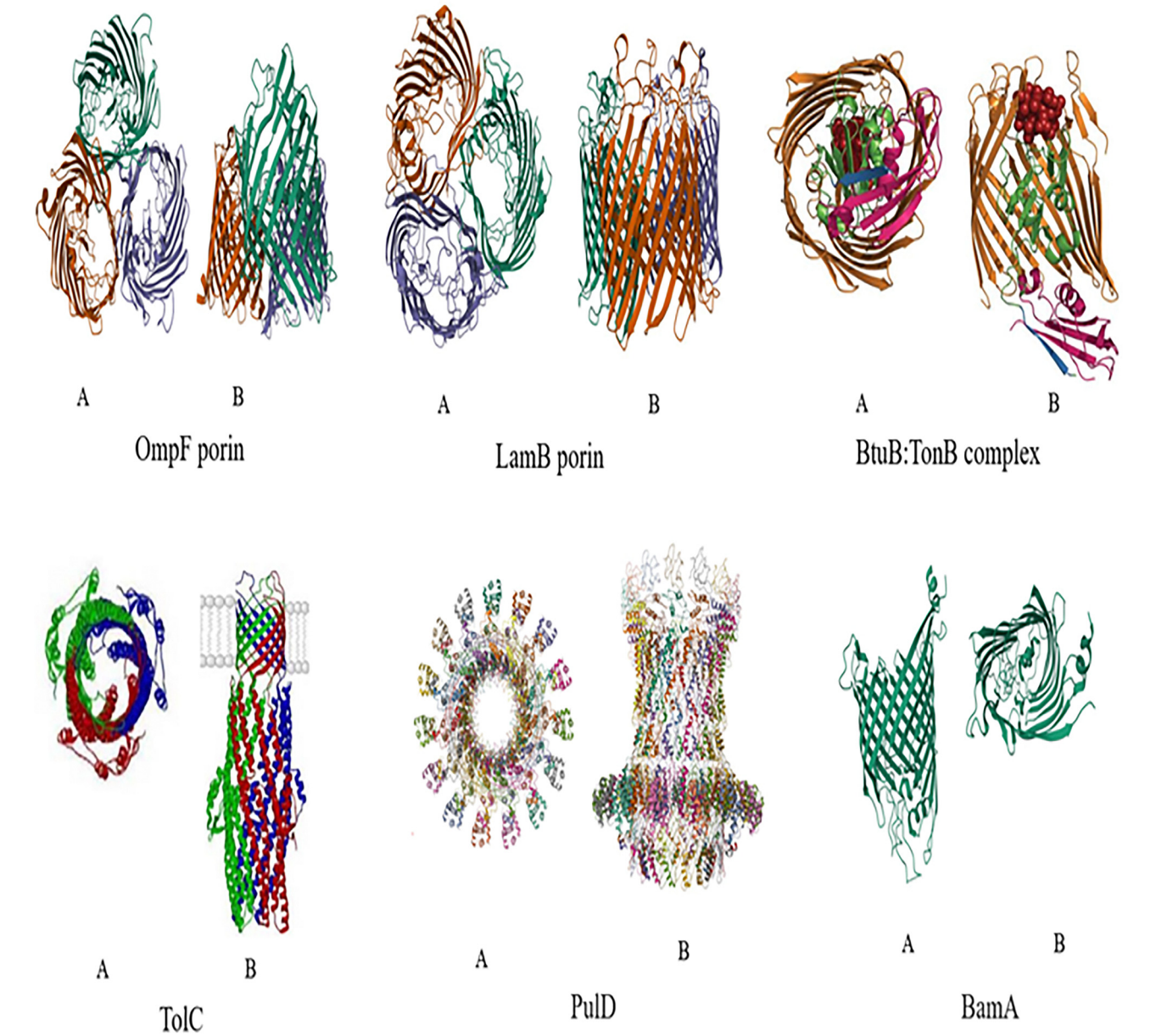

Fig. 11 Structure of some outer membrane proteins (https://www.rcsb.org/).

methicillin-resistant Staphylococcus aureus (*MRSA*), the hydrogel reduced bacterial viability by approximately 80%, attributed to the binding of MIPs to β-lactamase and inhibition of its hydrolytic activity. Such findings highlight the feasibility of employing MIPs to neutralise resistance-related enzymes.

In Gram-negative bacteria, the outer membrane acts as a protective barrier and organises key cellular functions. Outer membrane proteins (OMPs) with β-barrel structures, such as porins and other channels, facilitate the transport of ions, nutrients, and waste products, which is essential for bacterial metabolism and survival (Table 2 and Fig. 11). MIPs can be designed to specifically recognise these proteins,[145] and disrupt their functions, including permeability, structural integrity, virulence, and molecular transport.

Advanced approaches such as solid-phase imprinting[45] allow the use of purified proteins as templates to produce highly selective nano-MIPs. Similarly, snapshot imprinting[157,158] enables the identification of key peptide sequences that contribute to protein stability, which are then used as templates to generate nano-MIPs capable of recognising the full protein within the cell.[46]

In a recent study, snapshot imprinting was employed to map the surface proteome of lung cancer cells as a strategy for biomarker discovery. E. Piletska *et al.*[159] selectively captured peptides from proteins exposed on the surface of lung cancer cells using snapshot imprinting. By polymerising directly on live cells, the nanoMIPs enriched surface-accessible proteins, which were then identified by liquid chromatography-tandem mass spectrometry (LC-MS/MS). The study demonstrates a novel approach for profiling the cell surface proteome, providing potential biomarkers and targets for future cancer diagnostics and therapies.

Magumba *et al.*[160] employed a snapshot imprinting approach using MIPs to investigate differences in the cell-surface proteomes of three lung cancer cell lines (A549, H460, and H522) compared with a non-cancerous bronchial epithelial cell line (BEAS-2B). Proteomic analysis using LC-MS/MS identified hundreds of differentially expressed proteins (DEPs). Among these, the MIP-based approach enabled the identification of five key proteins (NPM1, TOP2A, EZH2, PRKDC, and HNRNPK) which are associated with lung cancer and may represent potential diagnostic biomarkers or therapeutic targets. These findings demonstrate the potential of nanoMIP-based snapshot imprinting as an alternative approach for identifying protein targets for diagnostic and therapeutic applications.

Snapshot imprinting can be exploited to systematically map outer membrane proteins (OMPs) and identify the most effective peptide sequences as templates for the synthesis of nano-MIPs *via* molecular imprinting. By precisely targeting these key protein sequences, the resulting nano-MIPs have the potential to selectively bind OMPs, thereby interfering with critical bacterial functions. This interference may compromise membrane permeability, disrupt structural integrity, attenuate virulence, and hinder the transport of essential molecules in coordination with inner membrane systems. Such a targeted approach offers a promising strategy for developing next-generation antibacterial materials with high specificity and efficacy.

Conclusion

This review describes recent advancements in the application of MIPs as antimicrobial agents, emphasising synthetic methodologies, therapeutic outcomes, and their broader implications for mitigating antimicrobial resistance (AMR). Current research demonstrates significant progress in engineering MIPs with high specificity and binding affinity for diverse bacterial targets. Notably, MIPs have proven effective as localised delivery vehicles for infections of the eye, skin, bone, and dental tissues. Furthermore, specialised MIPs have enhanced the efficacy of chloramphenicol through boron affinity and, when integrated with photothermal therapy, have achieved selective bacterial eradication by targeting lipopolysaccharides (LPS) to convert infrared energy into localised heat.

Beyond drug delivery, MIPs serve as robust abiotic receptors for sequestering LPS and inhibiting critical signalling molecules, such as quorum-sensing factors and alarmone nucleotides, thereby disrupting bacterial growth and intercellular communication. Structural integration with cryogels and nanofibers has further optimised these platforms by improving drug loading capacity and enabling sustained-release profiles. However, a more comprehensive characterisation of template–monomer complexes remains essential to elucidate the formation and spatial distribution of binding sites fully.

Future research must focus on the fundamental interactions between MIPs and bacterial biomarkers at the molecular level to clarify underlying binding mechanisms. The evidence suggests that outer membrane proteins in Gram-negative bacteria and β-lactamases in Gram-positive bacteria are prime templates for developing nano- and micro-MIPs. By targeting these vital structures, MIPs offer a transformative approach to bacterial neutralisation, providing a promising trajectory for innovative therapeutic and diagnostic solutions in the global fight against microbial resistance.

Conflicts of interest

There are no conflicts to declare.

Data availability

No primary research results, software or code have been included, and no new data were generated or analysed as part of this review.

Acknowledgements

The authors express gratitude for the doctoral scholarship from the Higher Committee of Education and Development in Iraq (HCED) awarded to A. Ibrahim.

Notes and references

1 R. C. Founou, L. L. Founou and S. Y. Essack, *PLoS One*, 2017, **12**, e0189621.
2 F. Prestinaci, P. Pezzotti and A. Pantosti, *Pathog. Glob. Health*, 2015, **109**, 309–318.
3 K. W. K. Tang, B. C. Millar and J. E. Moore, *Br. J. Biomed. Sci.*, 2023, **80**, 11387.
4 P. Dadgostar, *Infect. Drug Resist.*, 2019, 3903–3910.
5 A. Tačić, V. Nikolić, L. Nikolić and I. Savić, *Adv. Technol.*, 2017, **6**, 58–71.
6 K. M. Krause, A. W. Serio, T. R. Kane and L. E. Connolly, *Cold Spring Harbor Perspect. Med.*, 2016, **6**, a027029.
7 T. H. Grossman, *Cold Spring Harbor Perspect. Med.*, 2016, **6**, a025387.
8 M. Strieker and M. A. Marahiel, *ChemBioChem*, 2009, **10**, 607–616.
9 C. Foti, A. Piperno, A. Scala and O. Giuffrè, *Molecules*, 2021, **26**, 4280.
10 M. S. Butler, K. A. Hansford, M. A. Blaskovich, R. Halai and M. A. Cooper, *J. Antibiot.*, 2014, **67**, 631–644.
11 S. Reissier and V. Cattoir, *Expert Rev. Anti-Infect. Ther.*, 2021, **19**, 587–599.
12 N. Vázquez-Laslop and A. S. Mankin, *Trends Biochem. Sci.*, 2018, **43**, 668–684.
13 J. Spížek and T. Řezanka, *Biochem. Pharmacol.*, 2017, **133**, 20–28.
14 M. I. Hutchings, A. W. Truman and B. Wilkinson, *Curr. Opin. Microbiol.*, 2019, **51**, 72–80.
15 N. G. Bush, I. Diez-Santos, L. R. Abbott and A. Maxwell, *Molecules*, 2020, **25**, 5662.
16 G. L. Armstrong, L. A. Conn and R. W. Pinner, *JAMA*, 1999, **281**, 61–66.
17 G.-Y. Liu, D. Yu, M.-M. Fan, X. Zhang, Z.-Y. Jin, C. Tang and X.-F. Liu, *Mil. Med. Res.*, 2024, **11**, 7.
18 M. Vaara, *Front. Microbiol.*, 2019, **10**, 1689.
19 W. H. Organisation.
20 F. Malouin and L. Bryan, *Antimicrob. Agents Chemother.*, 1986, **30**, 1–5.
21 D. Sun, K. Jeannot, Y. Xiao and C. W. Knapp, *Front. Microbiol.*, 2019, **10**, 1933.
22 K. Tang and H. Zhao, *Infect. Drug Resist.*, 2023, 811–820.
23 G. Zhou, Q. Wang, Y. Wang, X. Wen, H. Peng, R. Peng, Q. Shi, X. Xie and L. Li, *Microorganisms*, 2023, **11**, 1690.
24 A. Farra, S. Islam, A. Strålfors, M. Sörberg and B. Wretlind, *Int. J. Antimicrob. Agents*, 2008, **31**, 427–433.
25 Z.-l Fang, L.-y Zhang, Y.-m Huang, Y. Qing, K.-y Cao, G.-b Tian and X. Huang, *Infect., Genet. Evol.*, 2014, **21**, 124–128.
26 M. Webber and L. Piddock, *J. Antimicrob. Chemother.*, 2003, **51**, 9–11.
27 B. Marquez, *Biochimie*, 2005, **87**, 1137–1147.
28 J. M. Munita and C. A. Arias, *Vir. Mech. Bact. Pathog.*, 2016, 481–511.
29 J. Lin, K. Nishino, M. C. Roberts, M. Tolmasky, R. I. Aminov and L. Zhang, *Front. Microbiol.*, 2015, **6**, 34.
30 T. M. Uddin, A. J. Chakraborty, A. Khusro, B. R. M. Zidan, S. Mitra, T. B. Emran, K. Dhama, M. K. H. Ripon, M. Gajdács and M. U. K. Sahibzada, *J. Infect. Publ. Health*, 2021, **14**, 1750–1766.
31 Y. Ma, F. Cai, Y. Li, J. Chen, F. Han and W. Lin, *Bioact. Mater.*, 2020, **5**, 732–743.
32 O. C. Farokhzad and R. Langer, *ACS Nano*, 2009, **3**, 16–20.
33 M. A. Beach, U. Nayanathara, Y. Gao, C. Zhang, Y. Xiong, Y. Wang and G. K. Such, *Chem. Rev.*, 2024, **124**, 5505–5616.
34 H. Bhardwaj, S. Sarthi and R. K. Jangde, *Pharm. Nanotechnol.*, 2025, DOI: 10.2174/0122117385366838250314110525.
35 N. Zhang, N. Zhang, Y. Xu, Z. Li, C. Yan, K. Mei, M. Ding, S. Ding, P. Guan and L. Qian, *Macromol. Rapid Commun.*, 2019, **40**, 1900096.
36 M. Włoch and J. Datta, *Comprehensive analytical chemistry*, Elsevier, 2019, vol. 86, pp. 17–40.
37 K. Flavin and M. Resmini, *Anal. Bioanal. Chem.*, 2009, **393**, 437–444.
38 A. G. Mayes and M. J. Whitcombe, *Adv. Drug Delivery Rev.*, 2005, **57**, 1742–1778.
39 K. Yoshimatsu, K. Reimhult, A. Krozer, K. Mosbach, K. Sode and L. Ye, *Anal. Chim. Acta*, 2007, **584**, 112–121.
40 J. Wang, P. A. Cormack, D. C. Sherrington and E. Khoshdel, *Angew. Chem.*, 2003, **115**, 5494–5496.
41 G. Zhao, J. Liu, M. Liu, X. Han, Y. Peng, X. Tian, J. Liu and S. Zhang, *Appl. Sci.*, 2020, **10**, 2868.
42 J. Yang, Y. Li, J. Wang, X. Sun, R. Cao, H. Sun, C. Huang and J. Chen, *Anal. Chim. Acta*, 2015, **872**, 35–45.
43 L. Wan, Z. Chen, C. Huang and X. Shen, *TrAC, Trends Anal. Chem.*, 2017, **95**, 110–121.
44 Q. Liu, J. Wan and X. Cao, *Process Biochem.*, 2018, **70**, 168–178.
45 F. Canfarotta, A. Poma, A. Guerreiro and S. Piletsky, *Nat. Protoc.*, 2016, **11**, 443–455.
46 S. S. Piletsky, A. Garcia Cruz, E. Piletska, S. A. Piletsky, E. O. Aboagye and A. C. Spivey, *Polymers*, 2022, **14**, 1595.
47 P. T. Vallano and V. T. Remcho, *J. Chromatogr. A*, 2000, **887**, 125–135.
48 M. Ovezova, F. Yılmaz, I. Göktürk, K. Ç. Güler and A. Denizli, *J. Pharm. Biomed. Anal. Open*, 2024, 100038.
49 J. Sarvutiene, U. Prentice, S. Ramanavicius and A. Ramanavicius, *Biotechnol. Adv.*, 2024, **71**, 108318.
50 A. Bossi, F. Bonini, A. Turner and S. Piletsky, *Biosens. Bioelectron.*, 2007, **22**, 1131–1137.
51 S. Scorrano, L. Mergola, R. Del Sole and G. Vasapollo, *Int. J. Mol. Sci.*, 2011, **12**, 1735–1743.
52 Y. Zhang, Q. Wang, X. Zhao, Y. Ma, H. Zhang and G. Pan, *Molecules*, 2023, **28**, 918.
53 H. Zhang, *Adv. Mater.*, 2020, **32**, 1806328.
54 L. Longo and G. Vasapollo, *Mini-Rev. Org. Chem.*, 2008, **5**, 163–170.
55 V. Pichon and F. Chapuis-Hugon, *Anal. Chim. Acta*, 2008, **622**, 48–61.
56 F. Tamayo, J. Casillas and A. Martin-Esteban, *Anal. Bioanal. Chem.*, 2005, **381**, 1234–1240.

57 F. Puoci, G. Cirillo, M. Curcio, F. Iemma, U. Spizzirri and N. Picci, *Anal. Chim. Acta*, 2007, **593**, 164–170.
58 C. Baggiani, L. Anfossi and C. Giovannoli, *Anal. Chim. Acta*, 2007, **591**, 29–39.
59 S. A. Piletsky, N. W. Turner and P. Laitenberger, *Med. Eng. Phys.*, 2006, **28**, 971–977.
60 W. Li and S. Li, *Oligomers-Polymer Composites-Molecular Imprinting*, Springer, 2007, pp. 191–210.
61 B. H. Abd, *Molecularly Imprinted Polymers for Drug Delivery*, University of Leicester, 2018.
62 L. Longo and G. Vasapollo, *Met.-Based Drugs*, 2008, **5**, 163–170.
63 Y. Ge and A. P. Turner, *Chem. – Eur. J.*, 2009, **15**, 8100–8107.
64 B. Tse Sum Bui, T. Auroy and K. Haupt, *Angew. Chem., Int. Ed.*, 2022, **61**, e202106493.
65 A. Aherne, C. Alexander, M. Payne, N. Perez and E. Vulfson, *J. Am. Chem. Soc.*, 1996, **118**, 8771–8772.
66 K. Ren and R. N. Zare, *ACS Nano*, 2012, **6**, 4314–4318.
67 H. Bao, B. Yang, X. Zhang, L. Lei and Z. Li, *Chem. Commun.*, 2017, **53**, 2319–2322.
68 Y. Long, Z. Li, Q. Bi, C. Deng, Z. Chen, S. Bhattachayya and C. Li, *Int. J. Pharm.*, 2016, **502**, 232–241.
69 M. Abdin, Z. Altintas and I. Tothill, *Biosens. Bioelectron.*, 2015, **67**, 177–183.
70 K.-I. Ogawa, M. Hyuga, T. Okada and N. Minoura, *Biosens. Bioelectron.*, 2012, **38**, 215–219.
71 R. Sulc, G. Szekely, S. Shinde, C. Wierzbicka, F. Vilela, D. Bauer and B. Sellergren, *Sci. Rep.*, 2017, **7**, 44299.
72 E. V. Piletska, G. Stavroulakis, L. D. Larcombe, M. J. Whitcombe, A. Sharma, S. Primrose, G. K. Robinson and S. A. Piletsky, *Biomacromolecules*, 2011, **12**, 1067–1071.
73 L. Ma, S. Feng, C. S. D. L. Fuente-Nunez, R. E. Hancock and X. Lu, *ACS Appl. Mater. interfaces*, 2018, **10**, 18450–18457.
74 S. Fa and Y. Zhao, *Bioorg. Med. Chem. Lett.*, 2019, **29**, 978–981.
75 J. G. Lopez, E. Piletska, M. Whitcombe, J. Czulak and S. Piletsky, *Chem. Commun.*, 2019, **55**, 2664–2667.
76 J. de Dieu Habimana, J. Ji, F. Pi, E. Karangwa, J. Sun, W. Guo, F. Cui, J. Shao, C. Ntakirutimana and X. Sun, *Anal. Chim. Acta*, 2018, **1031**, 134–144.
77 A. Motib, A. Guerreiro, F. Al-Bayati, E. Piletska, I. Manzoor, S. Shafeeq, A. Kadam, O. Kuipers, L. Hiller and T. Cowen, *Angew. Chem.*, 2017, **129**, 16782–16785.
78 W. Li, K. Dong, J. Ren and X. Qu, *Angew. Chem.*, 2016, **128**, 8181–8185.
79 M. A. R. Khan, A. R. A. Cardoso, M. G. F. Sales, S. Merino, J. M. Tomás, F. X. Rius and J. Riu, *Sens. Actuators, B*, 2017, **244**, 732–741.
80 X. Xue, J. Pan, H. Xie, J. Wang and S. Zhang, *React. Funct. Polym.*, 2009, **69**, 159–164.
81 Z. Wu, J. Hou, Y. Wang, M. Chai, Y. Xiong, W. Lu and J. Pan, *Int. J. Pharm.*, 2015, **496**, 1006–1014.
82 N. Malakooti, C. Alexander and C. Alvarez-Lorenzo, *J. Pharm. Sci.*, 2015, **104**, 3386–3394.
83 S. Kioomars, S. Heidari, B. Malaekeh-Nikouei, M. Shayani Rad, B. Khameneh and S. A. Mohajeri, *Pharm. Dev. Technol.*, 2017, **22**, 122–129.
84 V. Galván-Romero, F. Gonzalez-Salazar, K. Vargas-Berrones, L. E. Alcantara-Quintana, F. Martinez-Gutierrez, S. Zarazua-Guzman and R. Flores-Ramírez, *Eur. J. Pharm. Biopharm.*, 2024, **195**, 114178.
85 R. Khademi and M. Kharaziha, *ACS Appl. Mater. Interfaces*, 2024, **16**(25), 31966–31982.
86 Q. Hu, X. Chen, N. Zhao and Y. Li, *Mater. Lett.*, 2013, **106**, 452–455.
87 J. Kurczewska, M. Cegłowski, P. Pecyna, M. Ratajczak, M. Gajęcka and G. Schroeder, *Mater. Lett.*, 2017, **201**, 46–49.
88 M. Foroutan Koudehi and R. Zibaseresht, *Mater. Technol.*, 2020, **35**, 21–30.
89 E. Tamahkar, M. Bakhshpour and A. Denizli, *J. Biomater. Sci., Polym. Ed.*, 2019, **30**, 450–461.
90 H. Gong, W. Liu, M. Carlquist and L. Ye, *ChemBioChem*, 2019, **20**, 2991–2995.
91 Q. Zhang, M. Zhang, Z. Huang, Y. Sun and L. Ye, *ACS Appl. Polym. Mater.*, 2023, **5**, 3055–3064.
92 S. Shao, S. Gao, Y. Li and Y. Lv, *ACS Appl. Mater. Interfaces*, 2023, **15**, 16408–16419.
93 Y. Chen, Z. Zhang, Y. Chen, S. Zhou, Q. Deng and S. Wang, *J. Mater. Chem. B*, 2022, **10**, 9438–9445.
94 S. Diken Gür, M. Bakhshpour, N. Bereli and A. Denizli, *J. Biomater. Sci., Polym. Ed.*, 2021, **32**, 1024–1039.
95 H. Gong, S. Hajizadeh, W. Liu and L. Ye, *ACS Appl. Bio Mater.*, 2021, **4**, 2829–2838.
96 S. F. Elhabal, R. Abdelmonem, R. M. El Nashar, M. F. M. Elrefai, A. M. E. Hamdan, N. A. Safwat, M. S. Shoela, F. E. Hassan, A. Rizk and S. L. Kabil, *Pharmaceutics*, 2024, **16**, 947.
97 A. Mikagi, K. Manita, A. Yoyasu, Y. Tsuchido, N. Kanzawa, T. Hashimoto and T. Hayashita, *Molecules*, 2021, **27**, 256.
98 M. Jiang, A. N. Chattopadhyay, C. H. Li, Y. Geng, D. C. Luther, R. Huang and V. M. Rotello, *Chem. Sci.*, 2022, **13**, 12899–12905.
99 M. Santucci, F. Spyrakis, S. Cross, A. Quotadamo, D. Farina, D. Tondi, F. De Luca, J.-D. Docquier, A. I. Prieto and C. Ibacache, *Sci. Rep.*, 2017, **7**, 17716.
100 G. S. Weston, J. Blázquez, F. Baquero and B. K. Shoichet, *J. Med. Chem.*, 1998, **41**, 4577–4586.
101 P. C. Trippier and C. McGuigan, *MedChemComm*, 2010, **1**, 183–198.
102 A. F. Halbus, T. S. Horozov and V. N. Paunov, *ACS Appl. Mater. Interfaces*, 2019, **11**, 12232–12243.
103 H. M. U. Abid, M. Hanif, K. Mahmood, M. Aziz, G. Abbas and H. Latif, *ACS Omega*, 2022, **7**, 24415–24422.
104 A. Galstyan, R. Schiller and U. Dobrindt, *Angew. Chem., Int. Ed.*, 2017, **56**, 10362–10366.
105 Y. Hu, W. Huang, Y. Tong, Q. Xia and M. Tian, *New J. Chem.*, 2017, **41**, 7133–7141.
106 R. Xing, S. Wang, Z. Bie, H. He and Z. Liu, *Nat. Protoc.*, 2017, **12**, 964–987.
107 M. Peng, H. Xiang, X. Hu, S. Shi and X. Chen, *J. Chromatogr. A*, 2016, **1474**, 8–13.
108 X. Chen, Y. Liu, M. Zhong, J. Yang, Z. Lin and Y. Liang, *Anal. Sci.*, 2023, **39**, 13–22.

109 L.-x Ding, Y.-q Wang, X. Sun, Z.-q Jiang, X.-y Wang, Y.-f Zhou and X.-y Hou, *Anal. Methods*, 2023, **15**, 925–936.
110 S. Saito, T. L. Massie, T. Maeda, H. Nakazumi and C. L. Colyer, *Anal. Chem.*, 2012, **84**, 2452–2458.
111 A. C. V. Doughty, A. R. Hoover, E. Layton, C. K. Murray, E. W. Howard and W. R. Chen, *Materials*, 2019, **12**, 779.
112 L. Zhao, X. Zhang, X. Wang, X. Guan, W. Zhang and J. Ma, *J. Nanobiotechnol.*, 2021, **19**, 1–15.
113 H. Li, D. Yin, W. Li, Q. Tang, L. Zou and Q. Peng, *Colloids Surf., B*, 2021, **199**, 111502.
114 E. M. Peck and B. D. Smith, in *Synthetic Receptors for Biomolecules: Design Principles and Applications*, ed. B. Smith, The Royal Society of Chemistry, 2015.
115 V. C. Kalia, *Biotechnol. Adv.*, 2013, **31**, 224–245.
116 K. Papenfort and B. L. Bassler, *Nat. Rev. Microbiol.*, 2016, **14**, 576–588.
117 T. Defoirdt, G. Brackman and T. Coenye, *Trends Microbiol.*, 2013, **21**, 619–624.
118 A. V. Samrot, A. A. Mohamed, E. Faradjeva, L. S. Jie, C. H. Sze, A. Arif, T. C. Sean, E. N. Michael, C. Y. Mun and N. X. Qi, *Medicina*, 2021, **57**, 839.
119 E. Cavaleiro, A. S. Duarte, A. C. Esteves, A. Correia, M. J. Whitcombe, E. V. Piletska, S. A. Piletsky and I. Chianella, *Macromol. Biosci.*, 2015, **15**, 647–656.
120 J. Ashley, M.-A. Shahbazi, K. Kant, V. A. Chidambara, A. Wolff, D. D. Bang and Y. Sun, *Biosens. Bioelectron.*, 2017, **91**, 606–615.
121 E. V. Piletska, G. Stavroulakis, K. Karim, M. J. Whitcombe, I. Chianella, A. Sharma, K. E. Eboigbodin, G. K. Robinson and S. A. Piletsky, *Biomacromolecules*, 2010, **11**, 975–980.
122 D. K. Robinson and K. Mosbach, *J. Chem. Soc., Chem. Commun.*, 1989, 969–970.
123 E. V. P. J. Garcia Lopez, M. J. Whitcombe, J. Czulak and S. A. Piletsky, *R. Soc. Chem.*, 2019, **55**(18), 2664–2667.
124 T. Long, K. C. Tu, Y. Wang, P. Mehta, N. P. Ong, B. L. Bassler and N. S. Wingreen, *PLoS Biol.*, 2009, **7**, e1000068.
125 J. K. Hobbs and A. B. Boraston, *ACS Infect. Dis.*, 2019, **5**, 1505–1517.
126 V. Hauryliuk, G. C. Atkinson, K. S. Murakami, T. Tenson and K. Gerdes, *Nat. Rev. Microbiol.*, 2015, **13**, 298–309.
127 A. O. Gaca, C. Colomer-Winter and J. A. Lemos, *J. Bacteriol.*, 2015, **197**, 1146–1156.
128 K. Çetin, S. Aslıyüce, N. Idil and A. Denizli, *J. Biomater. Sci., Polym. Ed.*, 2021, **32**, 189–204.
129 S. A. Ragland and A. K. Criss, *PLoS Pathog.*, 2017, **13**, e1006512.
130 N. Khorshidian, E. Khanniri, M. R. Koushki, S. Sohrabvandi and M. Yousefi, *Front. Nutr.*, 2022, **9**, 833618.
131 L. Aminlari, M. Mohammadi Hashemi and M. Aminlari, *J. Food Sci.*, 2014, **79**, R1077–R1090.
132 B. Masschalck and C. W. Michiels, *Crit. Rev. Microbiol.*, 2003, **29**, 191–214.
133 B. Singh, K. Kim and M.-H. Park, *Nanomaterials*, 2021, **11**, 3411.
134 Y. Chen, X. Mu and F. Wang, *Polym. Sci., Ser. A*, 2018, **60**, 311–321.
135 P. S. Gungor-Ozkerim, T. Balkan, G. T. Kose, A. S. Sarac and F. N. Kok, *J. Biomed. Mater. Res., Part A*, 2014, **102**, 1897–1908.
136 A. J. Silvestre, C. S. Freire and C. P. Neto, *Expert Opin. Drug Delivery*, 2014, **11**, 1113–1124.
137 Y. Pötzinger, D. Kralisch and D. Fischer, *Ther. Delivery*, 2017, **8**, 753–761.
138 T. Li, M. Sun and S. Wu, *Nanomaterials*, 2022, **12**, 784.
139 M. F. Koudehi and S. M. Pourmortazavi, *Electroanalysis*, 2018, **30**, 2302–2310.
140 C. Tang, C. D. Saquing, J. R. Harding and S. A. Khan, *Macromolecules*, 2010, **43**, 630–637.
141 H. C. Williams, R. P. Dellavalle and S. Garner, *Lancet*, 2012, **379**, 361–372.
142 H. Gong, K. Zhang, C. Dicko, L. Bülow and L. Ye, *ACS Appl. Nano Mater.*, 2019, **2**, 1655–1663.
143 R. A. Bonomo, *Cold Spring Harbor Perspect. Med.*, 2017, **7**, a025239.
144 D. Meneksedag, A. Dogan, P. Kanlikilicer and E. Ozkirimli, *Comput. Biol. Chem.*, 2013, **43**, 1–10.
145 Y. He and Z. Lin, *J. Mater. Chem. B*, 2022, **10**, 6571–6589.
146 G. Kefala, C. Ahn, M. Krupa, L. Esquivies, I. Maslennikov, W. Kwiatkowski and S. Choe, *Protein Sci.*, 2010, **19**, 1117–1125.
147 K.-L. Lou, N. Saint, A. Prilipov, G. Rummel, S. A. Benson, J. P. Rosenbusch and T. Schirmer, *J. Biol. Chem.*, 1996, **271**, 20669–20675.
148 A. Charbit, *Front. Biosci.*, 2003, **8**, s265–s274.
149 T. Schirmer, T. A. Keller, Y.-F. Wang and J. P. Rosenbusch, *Science*, 1995, **267**, 512–514.
150 C. Balusek and J. C. Gumbart, *Biophys. J.*, 2016, **111**, 1409–1417.
151 T. Pieńko and J. Trylska, *PLoS Comput. Biol.*, 2020, **16**, e1008024.
152 V. Koronakis, *FEBS Lett.*, 2003, **555**, 66–71.
153 E. Freinkman, S.-S. Chng and D. Kahne, *Proc. Natl. Acad. Sci. U. S. A.*, 2011, **108**, 2486–2491.
154 K. Moehle, H. Kocherla, B. Bacsa, S. Jurt, K. Zerbe, J. A. Robinson and O. Zerbe, *Biochemistry*, 2016, **55**, 2936–2943.
155 M. T. Doyle and H. D. Bernstein, *Nat. Commun.*, 2019, **10**, 3358.
156 R. Albrecht, M. Schütz, P. Oberhettinger, M. Faulstich, I. Bermejo, T. Rudel, K. Diederichs and K. Zeth, *Acta Crystallogr. Sect. D: Biol. Crystallogr.*, 2014, **70**, 1779–1789.
157 S. S. Piletsky, E. Piletska, M. Poblocka, S. Macip, D. J. Jones, M. Braga, T. H. Cao, R. Singh, A. C. Spivey and E. O. Aboagye, *Nano Today*, 2021, **41**, 101304.
158 E. Piletska, D. Thompson, R. Jones, A. G. Cruz, M. Poblocka, F. Canfarotta, R. Norman, S. Macip, D. J. Jones and S. Piletsky, *Nanoscale Adv.*, 2022, **4**, 5304–5311.
159 E. Piletska, K. Magumba, L. Joseph, A. G. Cruz, R. Norman, R. Singh, A. F. Tabasso, D. J. Jones, S. Macip and S. Piletsky, *RSC Adv.*, 2022, **12**, 17747–17754.
160 K. Magumba, E. Piletska, T. H. Cao, D. Jones, S. Macip and S. Piletsky, *Polymers*, 2026, **18**, 281.

